



Modeling volcanic ash resuspension dynamics: the Eyjafjallajökull ash deposit case

Cameron R. Powell



**Faculty of Earth Sciences
University of Iceland
2018**

Modeling volcanic ash resuspension dynamics: the Eyjafjallajökull ash deposit case

Cameron R. Powell

60 ECTS thesis submitted in partial fulfillment of a
Magister Scientiarum degree in Geology

MS Committee
Throstur Thorsteinsson
Sara Barsotti

Master's Examiner
Guðrún Nína Petersen

Faculty of Earth Sciences
School of Engineering and Natural Sciences
University of Iceland
Reykjavik, October 2018

Modeling volcanic ash resuspension dynamics: the Eyjafjallajökull ash deposit case
Modeling volcanic ash resuspension dynamics
60 ECTS thesis submitted in partial fulfillment of a *Magister Scientiarum* degree in
Geology

Copyright © 2018 Cameron R. Powell
All rights reserved

Faculty of Earth Sciences
School of Engineering and Natural Sciences
University of Iceland
Tækniðarður – Dunhaga 5
107, Reykjavík
Iceland

Telephone: 525 4000

Bibliographic information:
Powell, Cameron R., 2018, *Modeling volcanic ash resuspension dynamics: the Eyjafjallajökull ash deposit case*, Master's thesis, Faculty of Earth Sciences, University of Iceland, pp. 71.

Abstract

The eruption of Eyjafjallajökull in early 2010 led to an increase in the frequency of observed PM₁₀ (particulate matter with diameter < 10 µm) resuspension events in the southern region of Iceland, attributed to the deposition of fresh volcanic tephra. Particulate matter under this diametric threshold is readily respirable by humans and livestock, and has been shown to cause adverse effects to human health and the agriculture and aviation industries. Improvements have been made to the processing of observational data from the time period of 23 May–2 July 2010, as well as to the scheme for calibration of the NAME Lagrangian dispersion model. A new method for calibration allowed for the derivation of a time-dependent scaling factor, representing the evolution of the source material as a function of time. The evolution of source material, due to various geomorphological and meteorological processes, affects its ability to be readily remobilized. Under the new calibration scheme, ash resuspension events in the immediate deposit proximity are captured 72% of the time, and those in the capital region to the southwest captured 57% of the time. This newly derived scaling factor indicates a rapid decline in volcanic ash resuspension following the end of an eruption event. The eruption signal dominates the record of observed PM₁₀ levels in the immediate weeks following an event end, after which the normal dust resuspension record dust returns, with only minor influence from the remaining volcanic ash.

*To Clarence Ostwald,
who demonstrated the value of hard work
and humor in the face of it.*

Table of Contents

List of Figures.....	xi
List of Tables	xiii
Acknowledgements.....	xv
1 Motivation	17
2 Background.....	19
2.1 Modeling Resuspension with NAME	19
2.2 Observations	20
3 Methodology.....	23
3.1 Selection of Data	23
3.2 Source Deposit Scaling.....	24
3.3 Calibration Methodology	25
3.3.1 Calculation of PM Background Levels.....	25
3.3.2 Removal of Large-scale Seasonal and Meteorological Effects.....	27
3.3.3 Time-dependent Calibration.....	28
4 Results	33
4.1 Glacier Source Removal	33
4.2 Data Comparison for the Period 23 May–2 July 2010	34
4.3 Data Comparison for the Period September 2010–February 2011.....	37
5 Discussion	41
5.1 Bulk Removal of Glaciers.....	42
5.2 Applicability to Other Deposits.....	43
6 Summary and Conclusions	45
References	47
Appendix A: Technical Aspects	51
A.1 Setup of Modeling Environment at IMO	51
A.2 Retrieval of Past NWP Data.....	52
A.3 Preprocessing of NWP Data.....	53
Appendix B: Supplementary Figures	55
Appendix C: Utilized Scripts	59
C.1 <i>scale_release.py</i>	59
C.2 <i>calibration_plot_only.py</i>	61
C.3 <i>subtractglaciers_glims.py</i>	67

Appendix D: Description of Input Files	71
D.1 <i>input.txt</i>	71
D.2 <i>sources.txt</i>	71
D.3 <i>MetDefnECMWF_OPER_0125_fore.txt</i>	71

List of Figures

Figure 1 Map showing the outline of the Eyjafjallajökull ash deposit considered in the numerical modeling; only locations with deposit thickness in excess of 0.5 cm were used. Also present are the locations of various meteorological and monitoring stations mentioned in this study.....	21
Figure 2 MODIS true color satellite imagery over Eyjafjallajökull on 16 September 2010 (left) and 19 September 2010 (right). Imagery from the intermediate time period displayed only full cloud cover (NASA Worldview).....	27
Figure 3 Comparison of observed PM ₁₀ concentrations and uncalibrated NAME model output for the monitoring stations at Grensásvegur and Heimaland. Each line represents the linear regression fit for corresponding observed and modelled values in a given time bin representing the number of days past the deposit eruption source end. The data points and corresponding linear fits for each time bin transition from red to blue the further away they occur from the eruption end.....	30
Figure 4 Daily calibration factors for the PM ₁₀ stations at Heimaland and Grensásvegur compared to the reciprocal of the time past eruption end. A linear regression line has been plotted through the data.....	31
Figure 5 Daily calibration factors for the PM ₁₀ stations at Heimaland and Grensásvegur compared to time past eruption end. Overlain is a plot representing the newly defined scaling factor K _t	32
Figure 6 Comparison between uncalibrated PM ₃₂ outputs at Drangslíðardalur using the source file representing the original areal extent (solid blue) and the source file modified to exclude all points covered by glaciers (dotted red).....	33
Figure 7 Comparison between observed PM ₁₀ concentrations at Heimaland (red) and scaled NAME model output (blue) at the same location. Dashed vertical lines represent each full week past eruption end.....	35
Figure 8 Comparison between observed PM ₁₀ concentrations at Grensásvegur (red) and scaled NAME model output (blue) at the same location. Below, a visualization of the 24-hour average direction from which wind was blowing at Tindfjöll shows directions assumed to not be conducive to transporting ash from Eyjafjallajökull to Grensásvegur in red. These same time periods are expressed on the comparison plot with green vertical bars. Dashed vertical lines represent each full week past eruption end.....	36
Figure 9 Comparison between observed PM ₁₀ concentrations at Grensásvegur (red) and scaled NAME model output (blue) at the same location. Below, a visualization of the 24-hour average direction from which wind was blowing at Tindfjöll shows directions assumed to not be conducive to transporting ash from Eyjafjallajökull to Grensásvegur in red. These same time periods are expressed on the comparison plot with green vertical bars.	

Dashed vertical lines represent each full week past eruption end. A dotted horizontal line at $50 \mu\text{g m}^{-3}$ exhibits the PM10 safety threshold.	37
Figure 10 Comparison between observed PM ₁₀ concentrations at Drangshlíðardalur (red) and scaled NAME model output (blue) at the same location. Dashed vertical lines represent each full week past eruption end.....	38
Figure 11 Schematic showing the effect of a change in source grid resolution. The bottom image (b) represents a grid where the edge size has doubled compared to that on the top (a), resulting in a particle release volume of four times the initial volume. In this scheme, NAME releases particles uniformly above the release area to a depth of 10 m	55
Figure 12 Schematic showing the division of a source grid cell into a triangle for the purposes of calculating surface area. Surface calculations were performed for each triangular half of the cell and were summed.....	56
Figure 13 PM ₁₀ measurements at Grensásvegur for all of 2009.....	56
Figure 14 MODIS true color satellite imagery over Eyjafjallajökull glacier on 9 July 2009 (top left), 25 May 2010 (top right), 2 June 2010 (bottom left), and 7 June 2010 (bottom right). The image from 2009 shows a relatively clear shot of the glacier prior to deposition of volcanic ash. The series from May–June in the remaining three images shows not only the relatively full coverage of the glacier in volcanic ash, but also the appearance and subsequent disappearance of snow over the area in the central region of the glacier, presumably above a particular altitude.	57
Figure 15 Map showing the isopach thickness of the Eyjafjallajökull tephra deposit (Gudmundsson et al., 2012).	58

List of Tables

Table 1 Available observation data.....	23
---	----

Acknowledgements

The author would like to thank the Icelandic Centre for Research (RANNIS) for the project and its funding; the University of Iceland, the Icelandic Met Office (IMO), and the UK Met Office for this collaborative research opportunity; the Environment Agency of Iceland and the University of Applied Sciences, Düsseldorf, Germany, for supplying the monitoring station data; Bogi Brynjar Björnsson for designing and finalizing the map in Figure 1; Sara Barsotti and Throstur Thorsteinsson for their guidance as thesis committee members; María Björk Gunnarsdóttir for her moral support and patience; and all whose financial support enabled this project to become possible in the first place. We acknowledge the use of imagery from the NASA Worldview application (<https://worldview.earthdata.nasa.gov/>) operated by the NASA/Goddard Space Flight Center Earth Science Data and Information System (ESDIS) project.

1 Motivation

Iceland regularly experiences episodes of airborne particulate matter—sand and dust of volcanic origin—due to its nearly 22 000 km² area of sandy desert available for wind-driven resuspension (Arnalds, 2010). Many of the recorded airborne particle events in Reykjavík may be traced back to these deserts and dust plume locations as the source (Thorsteinsson, Gísladottir, Bullard, & McTainsh, 2011).

Volcanic eruptions that deposit ash can exacerbate both the frequency and magnitude of resuspension events. In addition to providing a fresh surface source from which to remobilize particulate matter, volcanic ash itself yields a number of health and safety concerns. Particles with a diameter of 10 µm or less (PM₁₀) are readily respirable. Inhalation of material in this diameter range has been linked to cardiovascular and respiratory problems in humans, including the worsening of juvenile asthma (Braga, Zanobetti, & Schwartz, 2001; Dockery, Schwartz, & Spengler, 1992; Forbes, Jarvis, Potts, & Baxter, 2003). Volcanic ash also has the potential to yield toxic chemicals in its composition (Baxter, et al., 1999; Searl, Nicholl, & Baxter, 2002).

In addition to being hazardous to human health, airborne particulate matter of this size may affect both agriculture and aviation. Grazing animals have been shown to suffer from abrasion to tooth enamel and corneas, as well as to experience intestinal problems and potential starvation due to ash cover on vegetation; plant crops may be similarly affected (Wilson, Cole, Stewart, Cronin, & Johnston, 2011). Hazards to aircraft and airports during periods of ash remobilization rival conditions experienced during an ongoing eruption (Hadley, Hufford, & Simpson, 2003; Folch, Mingari, Osores, & Collini, 2014).

Following the eruption of Eyjafjallajökull in the south of Iceland that concluded on 22 May 2010, there was a notable increase in the frequency of resuspension events (Icelandic Meteorological Office, 2012; Thorsteinsson, Jóhannsson, Stohl, & Kristiansen, 2012). Later analysis of ash from this eruption determined that there was no present risk of toxic chemical composition (Damby et al., 2017). However, up to 20% of the estimated 384 ± 96 Tg of erupted material in the early phase of the eruption event fell below the PM₁₀ diametric threshold (Gudmundsson et al., 2012), causing a number of observed events through the remainder of the year during which PM₁₀ concentrations exceeded the European and Icelandic guidelines of 50 µg m⁻³ over 24 hours (European Parliament and Council, 2008; Böðvarsdóttir, 2008).

A joint venture between the Icelandic Meteorological Office (IMO), Institute of Earth Science at the University of Iceland, and UK Met Office provided a preliminary forecast warning system operated by the UK Met Office and using the Numerical Atmospheric-dispersion Modelling Environment (NAME) (Jones, Thomson, Hort, & Devenish, 2007; Leadbetter, Hort, von Löwis, Weber, & Witham, 2012). This was accomplished through the calibration of arbitrary model output to observed levels of particulate matter (PM). Doing so yielded a scaling factor K that, when applied to the model formula governing the source strength of the material flux from the surface, allowed for direct model output of PM concentrations in µg m⁻³.

Time-dependent factors affecting the properties of the source material—weathering and erosion, consolidation, compaction, bulk transport, plant growth, and burial in glacial ice—suggest that the scaling factor K would be a temporal relationship, evolving as a function of time, rather than being a simple static coefficient. Subsequent work expanding on the initial forecast calibration following a well-captured ash remobilization event in September 2013 offers supporting evidence for this; recalibration using this event resulted in a new scaling coefficient many orders of magnitude lower than that found previously (Beckett, Kylling, Sigurðardóttir, von Löwis, & Witham, 2017). Based on this assumption of a time-dependent scaling factor for model calibration, this project seeks to provide a better tool for and implementation of ash resuspension forecasting.

The aim of the following has been to recalibrate the model on a moving timeline and to design and implement various improvements to the forecast functionality. This has been accomplished through the reprocessing of available data from the initial time period of calibration, as well as examination of a longer continuous time period in the observational data for the purposes of model calibration goodness of fit.

For the purpose of this study, the NAME ash resuspension scheme has been implemented at the IMO to provide local daily forecasts of potential volcanic ash remobilization over Iceland. Methods for data processing in the calibration effort have been critically reviewed and modified, and the available data reprocessed accordingly. The relationship between observational data and uncalibrated NAME model output has been observed through a moving time frame, yielding a dynamic scaling relationship K_t that acts as a function of time from the end of a main eruption period. This analysis has been performed by modeling the ash resuspension events that occurred immediately after the 2010 Eyjafjallajökull eruption event (from 23 May–2 July 2010) and calibrating only on those due to the presence of the tephra deposit produced during this eruption.

2 Background

Wind blowing across a surface that contains unconsolidated sediment offers the potential for particle movement of varying type: rolling of larger particles (creep), bouncing of particles of more moderate size (saltation), and suspension of the smallest particles (Bagnold, 1941). This movement occurs only under certain conditions, when the wind speed at the surface exceeds a threshold velocity (Chepil, 1945). This wind threshold velocity is a factor reliant on a number of surficial, substance, and meteorological parameters (Fécan, Marticorena, & Bergametti, 1998; Gilette, Adams, Muhs, & Kihl, 1982). As the primary factor governing particle movement involves the interaction of wind only at the surface boundary, models typically regard only the wind velocity at the surface (called the friction velocity), and its relationship to a minimum value required for particle suspension (the threshold friction velocity).

2.1 Modeling Resuspension with NAME

The various methods used to calculate this threshold friction velocity involve physical parameters like surface roughness, soil moisture, and vegetation growth (Fécan et al., 1998; Marticorena & Bergametti, 1995). Given a lack of understanding of the local surface properties of the source area following the deposition of volcanic ash, existing dust remobilization schemes native to the NAME model were unable to be adapted to serve the modeling of ash resuspension (Leadbetter et al., 2012). An additional lack of sufficient data from the time period over the area precluded the team from employing a method by Draxler, Ginoux, & Stein (2010) by which they might derive values for threshold friction velocity based on aerosol optical depths. Experimentation with NAME ultimately allowed for an estimation of the appropriate surface friction velocity of 0.4 m s^{-1} (Leadbetter et al., 2012), later confirmed by a sensitivity analysis (Folch et al., 2014).

The source from which material is emitted is the areal extent of the Eyjafjallajökull ash deposit over land where the depth of erupted material is at least 5 mm thick (Figure 1) (Gudmundsson et al., 2012). It is represented in the model by an input file containing gridded points of latitude and longitude representing the center of $0.01^\circ \times 0.01^\circ$ degree cells. Each cell emits simulated particles uniformly within 10 m of the surface whenever the proper conditions are met at that location.

In the NAME resuspended ash scheme, material is released at a rate F proportional to the cube of the excess friction velocity:

$$F = \begin{cases} K(u_* - u_{*t})^3 & u_* \geq u_{*t} \\ 0 & u_* < u_{*t} \end{cases} \quad (1)$$

where u_* is the friction velocity in m s^{-1} , u_{*t} is the threshold friction velocity in m s^{-1} , and K is a dimensional constant giving the source strength units of g s^{-1} . As previously mentioned, K is the scaling factor yielding an actual source strength from the cube of the excess friction

velocity. K was initially set to 1 prior to model calibration. Particle release is also halted when precipitation exceeds the critical value of 0.01 mm h^{-1} .

2.2 Observations

Five stations providing hourly average PM_{10} measurements from a period between 23 May–2 July 2010 were in operation around the southern coast and the capital region of Reykjavík to the southwest (Figure 1). Two of these stations—one temporary monitoring station located in Hvolsvöllur and operated by the University of Applied Sciences, Düsseldorf, Germany, and the other a permanent Environment Agency of Iceland monitoring site at Hvaleyrarholt—yielded data from only one week each during the period of study.

A second permanent environment agency PM_{10} station at Grensásvegur in the capital region yielded the full set of data from all of 2009–2015. This monitoring station is situated at a busy urban intersection, yielding potentially higher background noise than more rural stations.

The remaining temporary PM_{10} station, run by the Environment Agency at Heimaland, was operational for nearly the entire duration from late May to early July. This location is placed much closer to the Eyjafjallajökull ash deposit, at a rural community center. Additional data from a fifth PM_{10} monitoring station at Kirkjubæjarklaustur, to the east of the source deposit, was made available for use by the Environment Agency.

The second type of monitoring data made available for this study comes from an optical particle counter (OPC) at Drangshlíðardalur in Skógar. Allowing for continuous measurements of the number of particles per liter of air within each of 31 diameter ranges from 0.25 to $32 \mu\text{m}$ (Leadbetter et al., 2012), this station produced a data time series from 21 September 2010 through 16 February 2011. These binned diameter ranges were converted into an overall mass concentration (in $\mu\text{g m}^{-3}$) given the assumptions of a uniform density of 2300 kg m^{-3} and perfect particle sphericity. Due to these assumptions, which are generally not the case during the eruption that lead to this deposit (Gislason et al., 2011), there is a degree of uncertainty in the PM_{32} mass calculations at this station.

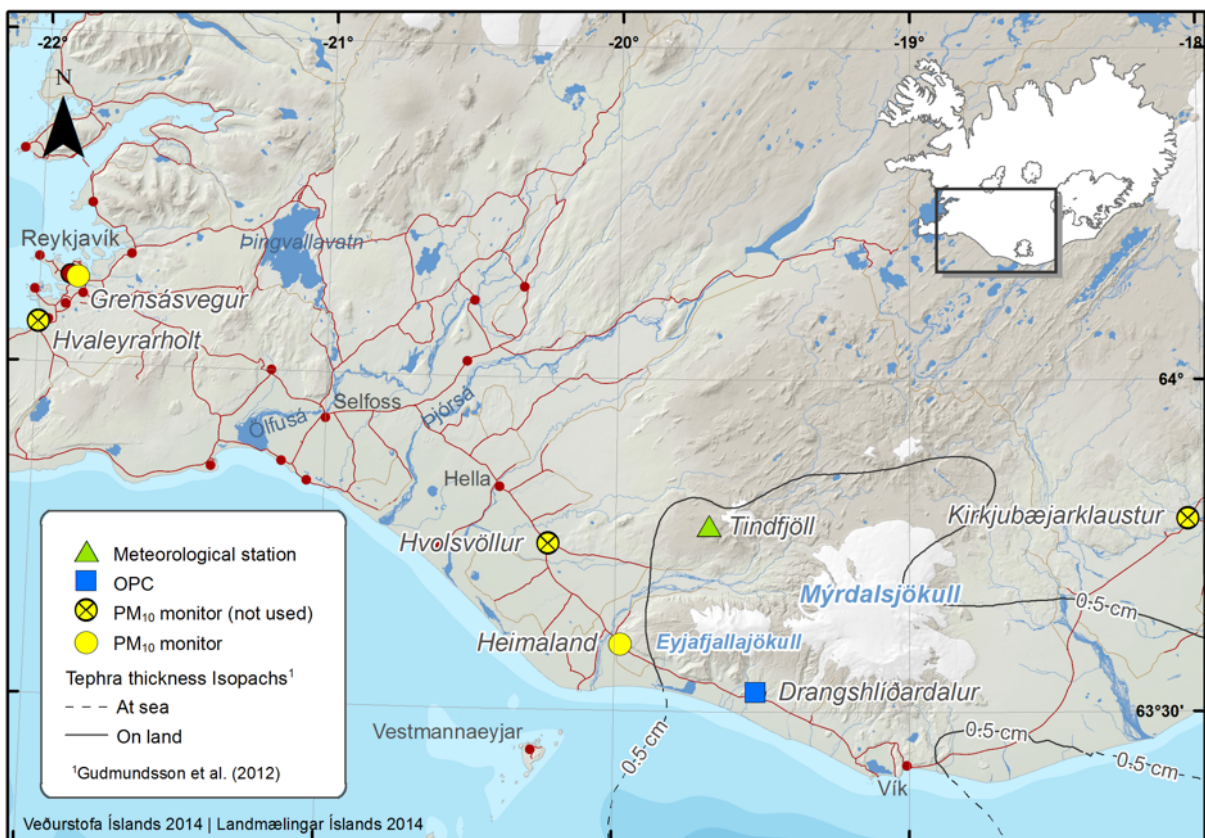


Figure 1 Map showing the outline of the Eyjafjallajökull ash deposit considered in the numerical modeling; only locations with deposit thickness in excess of 0.5 cm were used. Also present are the locations of various meteorological and monitoring stations mentioned in this study.

3 Methodology

The aim of this study has been to improve the methods used to prepare observational data to be directly compared with uncalibrated NAME model output, as well as to devise a scheme by which a temporally dependent scaling factor might be derived. The improvements in data processing have been accomplished through the following: discerning selection of data; implementation of a source scaling function that homogenizes the emitted material regardless of grid resolution; a new method for calculation of normal station mean background PM levels, eliminating the influence of suspension events from extraneous sources; and manual source processing to compensate for large-scale seasonal effects. The derivation of K as a dynamic scaling factor that is a function of time—rather than a static scaling coefficient as assumed previously—has been accomplished through analysis of static scaling values for a series of time bins following the eruption, followed by the subsequent derivation of a temporal relationship based on these values.

3.1 Selection of Data

Due to the short span of time from which observational data were available from the PM₁₀ stations at Hvaleyrarholt and Hvolsvöllur, both were removed from consideration during the calibration process. While small gaps were present in both the Heimaland data and observations from Grensásvegur during the selected time frames, the six-week time frame nevertheless was assumed to see sufficient coverage. In the later validation steps following model calibration, the gaps in data were properly accounted for.

Background PM₁₀ levels at the station at Kirkjubæjarklaustur were extraordinarily high, precluding its ability to be reliably applied to a calibration effort. Attempts to work with the data revealed a noise level incompatible with significant results, resulting in its removal in this study from consideration.

Table 1 Available observation data.

Name	Coordinates	Type	Duration	If used
Drangshlíðardalur	63.53°N, 19.52°W	OPC	21 Sept 2010–16 Feb 2011	Yes
Grensásvegur	64.13°N, 21.87°W	PM ₁₀	1 Jan 2009–31 Dec 2015	Yes
Heimaland	63.60°N, 19.98°W	PM ₁₀	26 May–2 July 2010	Yes
Hvaleyrarholt	64.06°N, 22.00°W	PM ₁₀	31 May–7 June 2010	No
Hvolsvöllur	63.75°N, 20.23°W	PM ₁₀	23–31 May 2010	No
Kirkjubæjarklaustur	63.79°N, 18.05°W	PM ₁₀	23 May–2 July 2010	No

Hvaleyrarholt and Hvolsvöllur excluded due to duration; Kirkjubæjarklaustur excluded due to data noise.

From the entire set of data obtained from the monitoring station at Grensásvegur, the full period from 23 May–2 July 2010 was selected, as was a section from 21 September 2010–16 February 2011 corresponding to the time period for which OPC data from Drangshlíðardalur was made available. The data from all of 2009 was additionally later used

in a discussion regarding observation of events unrelated to the recent deposition of volcanic ash.

3.2 Source Deposit Scaling

As mentioned previously, the source grid was set to emit a fixed amount of material per rectangular grid point under the appropriate meteorological conditions. Each rectangular cell of 0.01° latitude by 0.01° longitude centered on a coordinate had an emission rate of 1 g s^{-1} of resuspended ash, denoted in the input file containing the list of all source points making up the overall ash deposit. An early concern was in the scalability of the emission source grid resolution: if the size of each rectangular cell side were halved or doubled to accommodate a finer or more coarse resolution, for instance, the material emitted per grid area would theoretically quadruple or quarter, respectively (schematic shown in Figure 11 of Appendix B). A uniform emission rate per grid point based on degrees of latitude and longitude, however, has the second unintended effect that the same amount of resuspended material is emitted from a source point regardless of areal extent. As one moves from the equator toward the poles, lines of longitude converge, yielding a smaller surface area within the constraints set by the 0.01° by 0.01° boundaries. This would yield an observed net increase in released material per area with increased latitude. Both of these scaling obstacles may be rectified by considering that the assumed uncalibrated emission rate should be taken *per unit area*, rather than as a flat emission rate per grid point.

To accomplish such, it was first suggested that the coordinate system might be redefined. One might choose, for instance, to regenerate the sources file defining the source on a polar coordinate system centered on the Eyjafjallajökull deposit area. An alternative method was chosen, requiring scaling the emission rate for each grid point in the input file, such that the initial rate of 1 g s^{-1} resuspended ash be multiplied by the surface area of each grid cell. With this method it would be possible to scale any similarly constructed input file in the future, regardless of location or grid resolution.

Obtaining a scaled value for each quasi-rectangular cell involved dividing the cell diagonally between two corners and determining the values of each of the three angles within both respective half-cells (schematic shown in Figure 12 of Appendix B). This was accomplished for each angle through the calculation of the bearing from the central point of each angle to each of the respective ends, adapting into a Python script the following formula to find the bearing θ in radians:

$$\theta = \text{atan2}(\sin \Delta\lambda \cdot \cos \varphi_2, \cos \varphi_1 \cdot \sin \varphi_2 - \sin \varphi_1 \cdot \cos \varphi_2 \cdot \cos \Delta\lambda) \quad (2)$$

where φ and λ represent latitude and longitude in radians, respectively (Veness, 2017). The difference between the two resulting bearings was taken in each case, yielding a value for each internal angle within the triangle. Following each angle determination within the half-cell triangle, the surface area Δ of the spherical triangle was calculated given an assumed mean Earth radius R of approximately 6371 km (Moritz, 2000) and the following relationship:

$$\Delta = R^2[(A + B + C) - \pi] \quad (3)$$

where A, B, and C are the three internal angles of the spherical triangle (Gellert, Gottwald, Hellwich, Kästner, & Künstner, 1989).

It is also assumed here that the surface of the Earth is smooth, and that the calculation of surface area is therefore largely unaffected by local geology.

The major drawback to utilizing this particular method to scale the sources input file lies in the necessity that the bearing calculations determining the angles be operating under the assumption that the path between points follows a great circle. In reality, all lines of latitude aside from the equator do not follow such a path. The surface area will therefore ultimately be miscalculated to a certain degree, though with the assumption that the systematic over- and underestimation at the northern- and southernmost borders of each grid square will yield a net error small enough to be negligible on the larger scale.

Based on the above, a Python script was written that would parse an input file of source points, and apply the above transformation for a 0.01° by 0.01° cell centered on each given latitude-longitude coordinate (Appendix C.1). Following the bulk scaling of this sources file, the northernmost point of the ash deposit yielded an emission rate of 0.54 g s^{-1} at 63.87°N latitude, a total emission rate roughly 1.8% smaller than 0.55 g s^{-1} at the southernmost point of 63.40°N latitude.

3.3 Calibration Methodology

3.3.1 Calculation of PM Background Levels

To determine the normal background level for each monitoring station, the mean and standard deviation of each data set were determined. Significant statistical outliers to the mean were then removed from the data, and the entire process was repeated iteratively (recalculating mean and standard deviation on the new data set) until all observations were within statistically significant agreement. This iterative method was chosen over a simpler single removal of outlying data points in order to account for the removal of the remnant trunks from extraneous resuspension events. Following the initial culling of the aberrant events, elevated PM concentrations would still remain in the periods leading up to and following the event peaks, still positively skewing the resulting calculation of the mean, as well as yielding a larger standard deviation.

This method was chosen to improve upon the initial approach involving the simple procedure of averaging PM_{10} concentrations during the study time period when no resuspended ash was predicted at the location by NAME, as performed by Leadbetter et al. (2012). This prior method for calculating background values assumes a perfect model fit at the outset. However, the goodness of fit analysis performed in this prior study suggest that only 66% of events were properly captured by NAME. The model output did not sufficiently describe the events present in the observational data, making its application toward background value calculation not appropriate. In addition, this preliminary work demonstrated that specific events could be offset by several hours. Such a temporal offset would also allow for actual resuspension events that had been predicted by the calibrated model (and therefore included in the hit rate calculation) to nevertheless be captured by the background level calculation method.

The above new method for calculation of station background values is intended to eliminate all airborne particulate matter events from the calculation. Hourly PM₁₀ measurement data was obtained from the Environment Agency of Iceland for the station at Grensásvegur for all of 2009–2015. Visual inspection of the period of all of 2009 shows numerous events throughout the year of airborne particulate matter at this station (Figure 13 in Appendix B). These events all predate the eruption of Eyjafjallajökull, and therefore are entirely unrelated to the deposited source of ash in the south of Iceland. The largest of these events at Grensásvegur reaches a peak concentration of 650 µg m⁻³ in mid-May 2009. While this event is lower than the maximum observed post-eruption event, it nevertheless represents a significant level above the standard background. As such, and due to the nature of the temporal calibration discussed below, inclusion of these events in the background level calculation would yield a systematic under-estimation of the value of K at any given time.

Similarly, possible inclusion of additional events in the background calculation in the earlier study due to NAME under-prediction of ash resuspension is precluded by the fact that the goodness of fit of the model possessed a mutual dependence on this calibration method. NAME was first employed to determine PM₁₀ background values, which were then fed back into the model calibration used to determine the scaling coefficient, which was again later used to assess the initial suitability of the model. This dependency of the original background calculation on model goodness of fit requires an independent method by which normal background levels could instead be computed. The benefit of utilizing this new method is in its removal of high-magnitude events that lie outside the typical background level, and are otherwise not regular in period, duration, or magnitude.

There are drawbacks to this iterative method for background calculation. Due to inherent randomness, the systematic removal of outlying values following the bulk removal of larger-scale events leaves the perceived normal background value prone to underestimation. Naturally variable data points have the potential to be selected for removal, artificially lowering the mean past the intended end point of the iterative process. This behavior occurred in practice when calculating the average background levels of airborne particulate matter at Drangshlíðardalur. The location of this monitoring station within the volcanic ash deposit was likely a contributing factor to increased noise levels in the data, due to an increased ability for common or regular processes to readily yield remobilization. Following the above process of iterative noise removal intended to yield a background PM₃₂ average, the data became processed to too fine a degree, filtering out a significant portion of what was likely valid data for the station.

To remediate this underestimation of background PM₃₂ levels at Drangshlíðardalur, the background from the next nearest observation station was used as a rough approximation of regular conditions. Heimaland, roughly 24 km away from the OPC station, had both its observational data and background levels calculated to only represent the local levels of PM₁₀, necessitating a conversion to allow for the extended particle range detected at Drangshlíðardalur. The particle size distribution from the Eyjafjallajökull eruption (Gislason et al., 2011) allowed for a relationship for the ratio of deposit PM₁₀ to PM₃₂ to be estimated. This scaling ratio was then applied to the calculated background level at Heimaland, effectively approximating the average background PM₃₂ level, assuming an effective uniform distribution of particulate matter during remobilization events of this magnitude.

3.3.2 Removal of Large-scale Seasonal and Meteorological Effects

One of the anticipated time-dependent causes of decreased material availability was the covering of a large portion of the ash deposit due to snowfall on the underlying glaciers. Manual inspection of the source area using MODIS true color satellite imagery revealed a snowfall event between 16 September and 19 September 2010 that led to this mass covering of source ash. Subsequent satellite image coverage of this location indicate that this snow cover resulted in a permanent removal of this section of the ash deposit (Figure 2). Due to both the seasonality of this covering of source deposit and the resolution of the scale on which it occurs, it was deemed appropriate to account for this mass removal manually, so as to not improperly skew the eventual calculation of a temporally dependent scaling relationship.

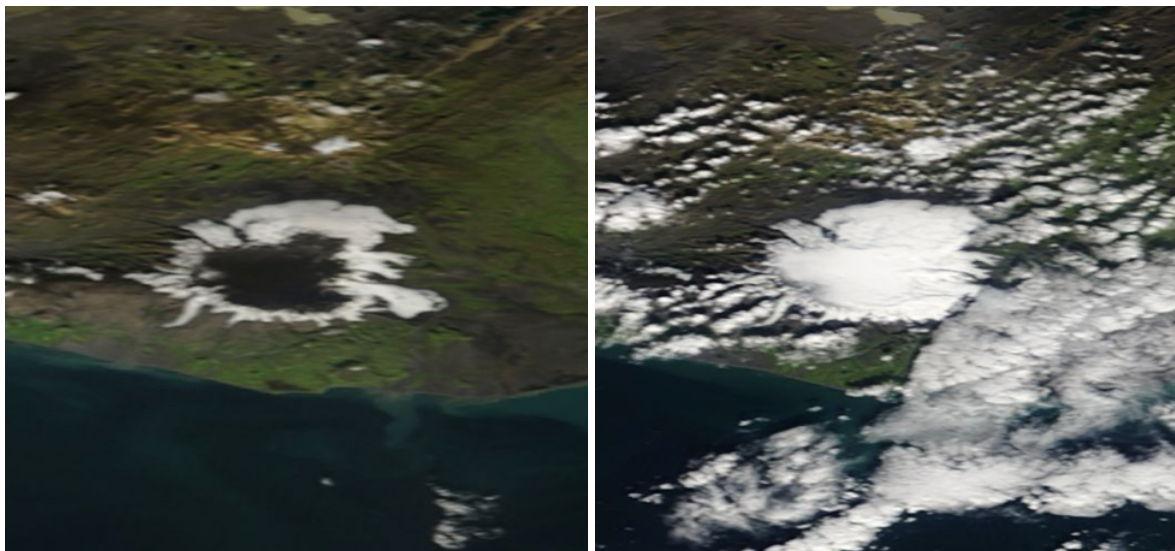


Figure 2 MODIS true color satellite imagery over Eyjafjallajökull on 16 September 2010 (left) and 19 September 2010 (right). Imagery from the intermediate time period displayed only full cloud cover (NASA Worldview).

To accomplish this bulk removal due to glacially located snowfall, a Python script was written that filtered the sources file and removed the appropriate points. Glacial extent was approximated by a polygon shape file of all glaciers over Iceland (Sigurdsson, 2005). Due to the uncertainty in the actual areal extent of snowfall on the glacier, this method is considered to only roughly approximate the conditions after the period of snow accumulation. However, due to the overall size of the area of removal, it is assumed that unknown error regarding the behavior at the periphery of the glacier is lower than the effect of removing from the sources file the glacier as a whole.

Given the historical record of airborne particulate matter events at Grensásvegur prior to the Eyjafjallajökull eruption, an attempt was made to filter out events originating from extraneous sources. This was accomplished through the retrieval of average wind directions from the meteorological station at Tindfjöll (Figure 1). This station is on the western periphery of the source deposit considered for resuspension, and is roughly in line with the

monitoring station at Grensásvegur in relation to the center of the source. It was assumed that when average wind directions at Tindfjöll originating from a 90° wedge roughly facing Grensásvegur (from 245° to 335°) were present, observed airborne particulate matter at the PM₁₀ station would be unlikely (though still possible) to have originated from the source deposit in question, and would thus be excluded from consideration during analysis of the goodness of fit of the calibrated model.

3.3.3 Time-dependent Calibration

Prior research on the resuspension characteristics of volcanic ash in the south of Iceland has acknowledged the assumption that various time-dependent processes are likely to have an effect on the remobilization of ash from the source deposits (Leadbetter et al., 2012; Beckett et al., 2017; Liu et al., 2014). This temporal scaling relationship is assumed to arise due to various geomorphological and meteorological processes acting on the source material: cementation, compaction, erosion, dispersion, and re-deposition of sediment, as well as source cover by new plant growth or snow.

Due to the uncalibrated nature of the processing done by NAME in this study, tracking of material removal and re-deposition is not feasible. While theoretically possible given a known source emission rate, the aim of this project is to calibrate the source emission rate, effectively making the process of tracking these spatial changes and calibrating the model output mutually dependent. It is therefore then assumed that material removal from the source deposit will be accounted for in the calibration relationship, and the emergence of new source locations due to re-deposition will be ignored. This assumption also then necessitates that the effect of ash removal contributes to the decrease of resuspension potential of the source as a whole, rather than allowing for inhomogeneity in the source evolution.

Other large-scale seasonal effects besides glacial snowfall that affect the ability for the remobilization of source material have not been accounted for. These include the spatial and seasonal extent of plant regrowth, as well as seasonal variations in precipitation potentially causing varying rates of sediment evolution. For the purposes of deriving a temporal calibration relationship, the short time interval and single eruption event on which calibration was performed preclude the ability to study potential seasonal variation.

Under the assumption that a given ash deposit following an eruption event represents a finite and non-renewable source of ash available for remobilization, one may assume that any and all processes acting on the source that change the ability for particles to be resuspended must not decrease the calibration scaling factor below zero, else it would suggest that NAME output values would ultimately yield the bulk remobilization of a negative mass of source ash. This, coupled with the assumption that the ability for the source material to be resuspended decreases as some function of time (Leadbetter et al., 2012; Beckett et al., 2017; Liu et al., 2014), lends itself to the hypothesis that a time-dependent and decreasing scaling factor applied during the calibration of NAME output must approach some asymptote as time increases to infinity.

Obtaining such an asymptotic relationship required independent analysis of a scaling coefficient K for multiple time-binned intervals following the end of the Eyjafjallajökull eruption sequence. The chosen duration for each time bin was one day, and each of the two stations involved in the calibration (Grensásvegur and Heimaland) were treated separately.

For each station and time bin, observed concentrations of airborne particulate matter were compared to NAME output when the observations exceeded the daily $50 \mu\text{g m}^{-3}$ limit and when there was any amount of predicted material in the model output (Figure 3). The scaling coefficient for each time bin was taken to be the slope of a regression line through the data. Data and regression lines immediately following the eruption end are represented by red coloration, which transitions to blue as time bins occur further from the eruption end. This method differs from the method used previously in that it requires some level of particulate matter predicted by NAME, aiming to reduce the error introduced to the calibration by events from other particle sources, as well as eliminate any bias due to lack of goodness of fit of the resuspension scheme in NAME.

Prior to the plotting of observational data, the normal particle background values were subtracted from the observational data. Subtraction of such a value was necessary so as to avoid overestimating the value for the daily scaling factor K by including normal levels of suspended particulate matter from other sources. Additionally, only observed values that were initially more than two standard deviations above the mean at each station were considered for analysis, to allow for relative certainty that elevated values were in fact present.

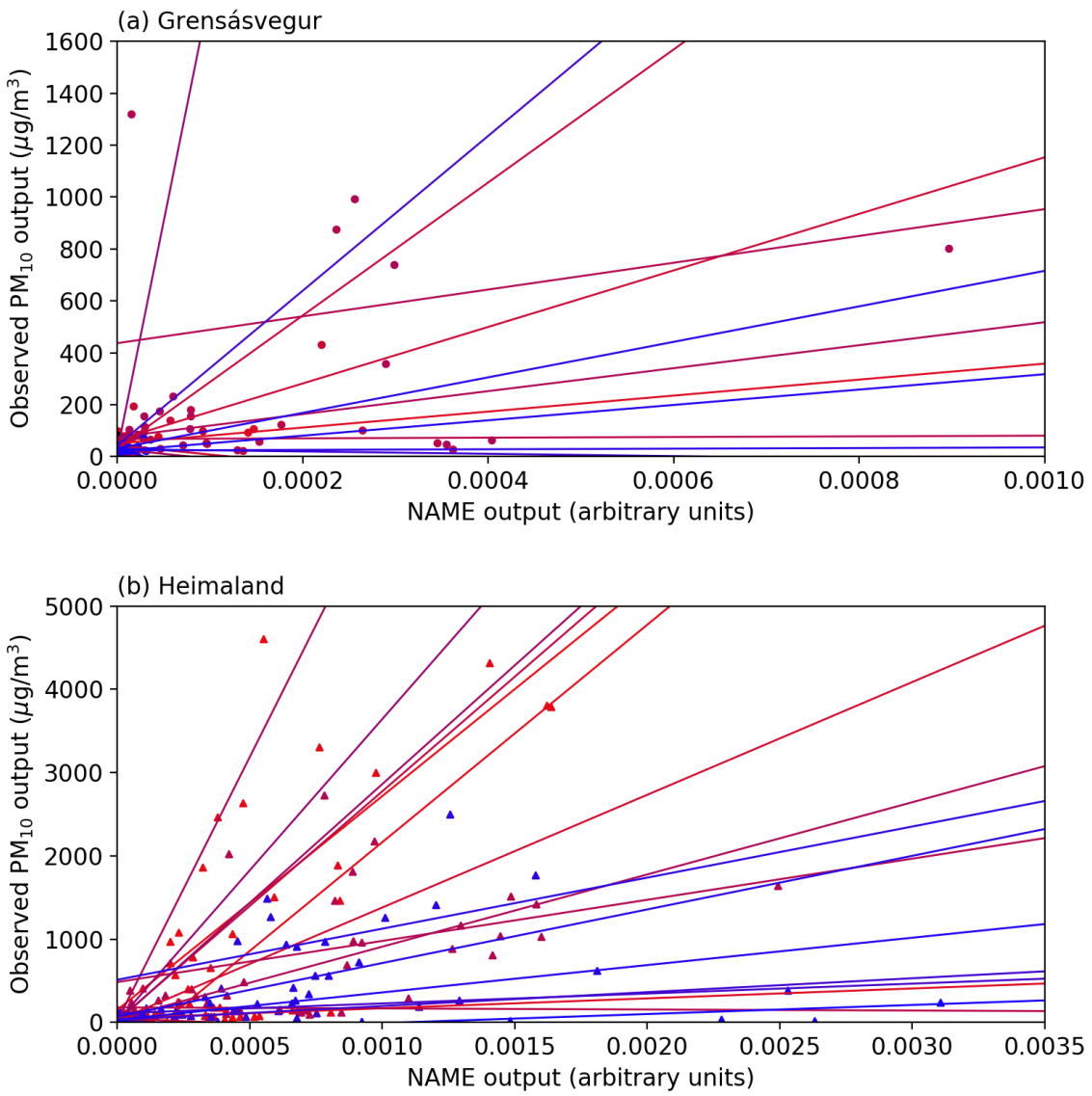


Figure 3 Comparison of observed PM₁₀ concentrations and uncalibrated NAME model output for the monitoring stations at Grensásvegur and Heimaland. Each line represents the linear regression fit for corresponding observed and modelled values in a given time bin representing the number of days past the deposit eruption source end. The data points and corresponding linear fits for each time bin transition from red to blue the further away they occur from the eruption end.

Due to the nature of the occasional temporal offset of observed versus modelled events, wherein model peaks and actual observed peaks would sometimes differ in timing by up to several hours, a number of individual K analyses (derived from the slope of the linear regression through the plotted points from a given time bin) resulted in negative values. These were primarily a result of such offset peaks yielding observational concentrations when there was little model output, and likewise capturing smaller observed values during moments of elevated model output. A positive linear regression through this data anchored at or near the origin might have theoretically yielded an appropriate positive slope as if the event peaks had properly overlapped. However, regression lines drawn through this data with no anchor point instead resulted in improperly negative slopes. An inability to

satisfactorily resolve this regression line difficulty resulted in the data from those particular time bins and locations ultimately removed from overall consideration in the calibration process.

Despite the above precautions, a number of statistical outliers in the data remained. It is possible that these were due to a variety of reasons. Observed events originating partially or wholly from alternative sources of airborne particulate matter may have contributed to artificially inflated values for K , as well as the potential effect of offset events spanning the cutoff threshold between time bins (i.e.: if an observed event peaked at 22:00 and the model instead predicted a peak at 02:00 the following day, these data would be split between two different time bins, skewing the resulting calculation of K for each bin). Minor artifacts introduced during the preprocessing of the numerical weather prediction files (Appendix A.3) may also have been a contributing factor.

These obvious outliers were manually removed through an iterative method similar to that used to derive the background values for each monitoring station. For each day within the extent of the observational data from Heimaland and Grensásvegur (immediately following the eruption), the calculated value for K at each station and in each respective time bin was plotted. A linear regression was plotted through the data, as well as the 99% prediction interval field. Points lying outside the bounds were assumed to be the result of unknown error from the variety of reasons discussed above, and were subsequently removed.

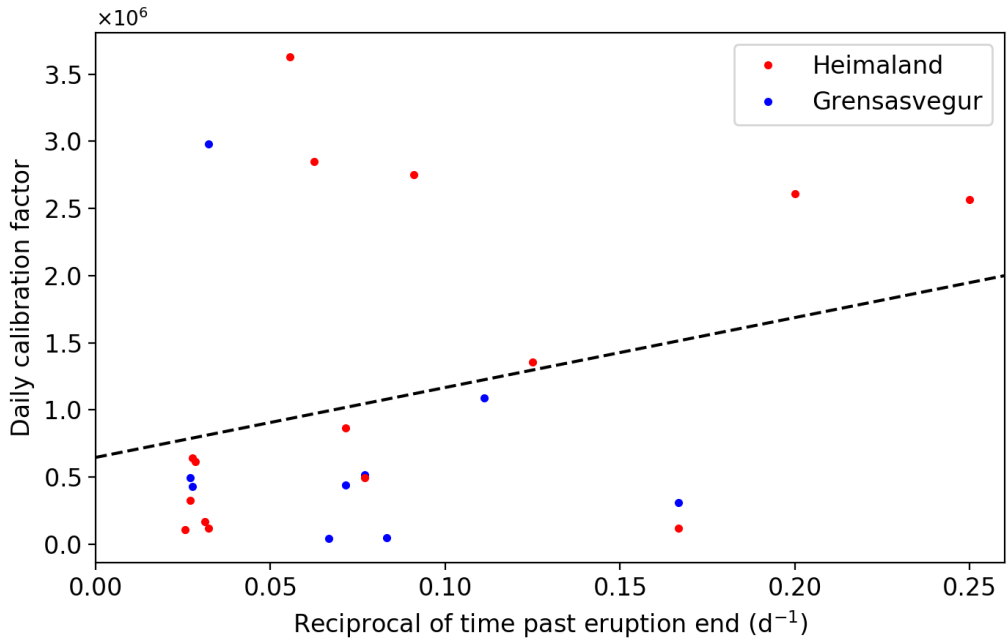


Figure 4 Daily calibration factors for the PM₁₀ stations at Heimaland and Grensásvegur compared to the reciprocal of the time past eruption end. A linear regression line has been plotted through the data.

The assertion that a temporal decrease in the scaling factor would ultimately approach an asymptote resulted in the necessity to regard the data as an inverse function of time. The

calculated daily values for K were plotted over the inverse of the number of days past the eruption for each time bin, and a linear relationship determined (Figure 4). The new calibration scaling factor K_t was taken to be a function of the slope of this regression line and its intercept at $f(1/t) = 0$, where t is the number of days past the end of the eruption period. Here, $K_t = 5.21 \times 10^6 t^{-1} + 6.5 \times 10^5$ (Figure 5). NAME prediction outputs for each station were scaled accordingly.

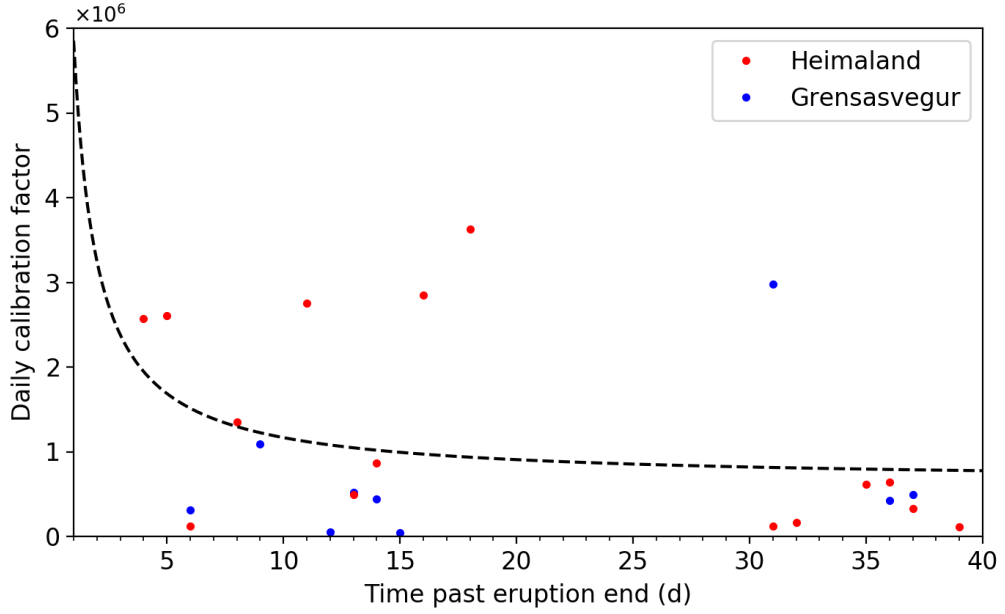


Figure 5 Daily calibration factors for the PM_{10} stations at Heimaland and Grensásvegur compared to time past eruption end. Overlain is a plot representing the newly defined scaling factor K_t .

4 Results

4.1 Glacier Source Removal

Following the bulk removal of source material in the deposit area via the glacial polygon overlap, NAME was run to output uncalibrated PM₃₂ at Drangshlíðardalur both with the original source file and with the newly reduced source. Based on the number of grid points removed from the original total, the overall source decreased in size by approximately 21.7%. Due to the timing of the event, between 16–19 September 2010, the effect of this removal was apparent upon inspecting the NAME output at Drangshlíðardalur over the period of time from 21 September 2010–17 February 2011, having run the model both with and without the removal of source material (Figure 6).

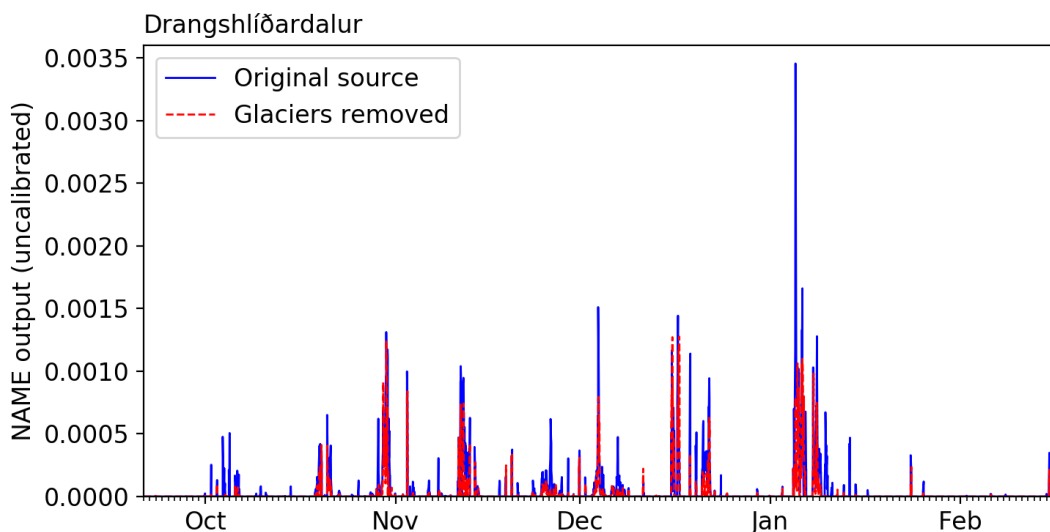


Figure 6 Comparison between uncalibrated PM₃₂ outputs at Drangshlíðardalur using the source file representing the original areal extent (solid blue) and the source file modified to exclude all points covered by glaciers (dotted red).

With NAME set to model concentrations of PM₃₂ at this monitoring station (matching the particle diameters observed by the OPC), the uncalibrated cumulative sum of observed particulate matter output by the model decreased by 46.3% following the removal of only 21.7% of the source deposit. The variations in event magnitude and duration are not uniform, indicating a dependence on wind direction. A plot of the time series of both pre- and post-glacier removal uncalibrated model concentrations exhibits the variance in the output at Drangshlíðardalur.

Many of the small-scale events in this time period, particularly those observed between 30 September–6 October 2010, are drastically reduced in magnitude. Medium-scale events on 12 December 2010 and 8 January 2011 see a decrease in peak magnitude of roughly half following the removal of source material. The largest event, on 5 January 2011, has its peak magnitude quartered. Two modelled events, on 29–30 October 2010 and 15–16 December 2010, actually exhibit a small increase in peak magnitude.

4.2 Data Comparison for the Period 23 May–2 July 2010

Observational data has been plotted alongside NAME output concentrations, to compare timing and magnitude of resuspension events. Prior to both visualization and the subsequent goodness of fit calculations, the previously calculated background levels at each station have been systematically subtracted from the observations. In the cases where this subtraction yielded negative values, they were instead taken to be zero, to better facilitate temporal averaging (as no perceived detection of airborne particulate matter would ever result in a negative value for concentration). The NAME outputs have all had the newly derived scaling factor K_t applied.

Hit rates and false alarm rates (Stephenson, 2000) have been calculated here only for Heimaland and Grensásvegur. 24-hour rolling averages of concentrations were performed on the observational data and scaled model output, taking the average daily concentration above $50 \mu\text{g m}^{-3}$ to be the basis for categorization as an event. Under these parameters, episodes of high PM_{10} concentration are considered to be when the 24-hour average concentration exceeds that threshold, rather than simply when any momentary observation exceeds $50 \mu\text{g m}^{-3}$.

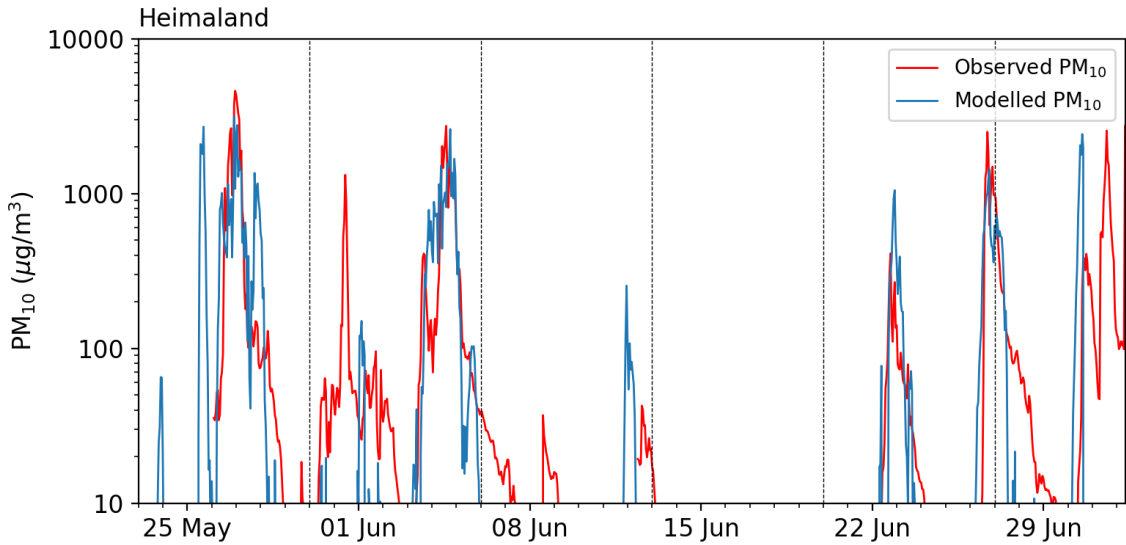


Figure 7 Comparison between observed PM₁₀ concentrations at Heimaland (red) and scaled NAME model output (blue) at the same location. Dashed vertical lines represent each full week past eruption end.

Episodes of high PM₁₀ concentration occurred at Heimaland on 26–29 May, 30 May–2 June, 2–6 June, 21–23 June, 25–28 June, and 29 June–2 July (Figure 7). The hit rate and false alarm rate were 71.9% and 2.6%, respectively. Notable is that data prior to 26 May is absent from the Heimaland observations, in addition to the minor gaps in the data noted previously (see Section 3.1). With respect to the model predictions where they overlay available observational data, the calibrated NAME output appears to agree fairly well in both timing and magnitude, with notable exception to the model absence of the large observational peak on 31 May. Some of the predicted events do appear to exhibit truncation, though this had previously been attributed to the sharp cut-off of resuspension below the threshold friction velocity (Leadbetter et al., 2012). PM₁₀ concentrations reached a maximum of 4605 µg m⁻³ at Heimaland on 26 May 2010, slightly underestimated by the calibrated model prediction of 3154 µg m⁻³ the hour prior.

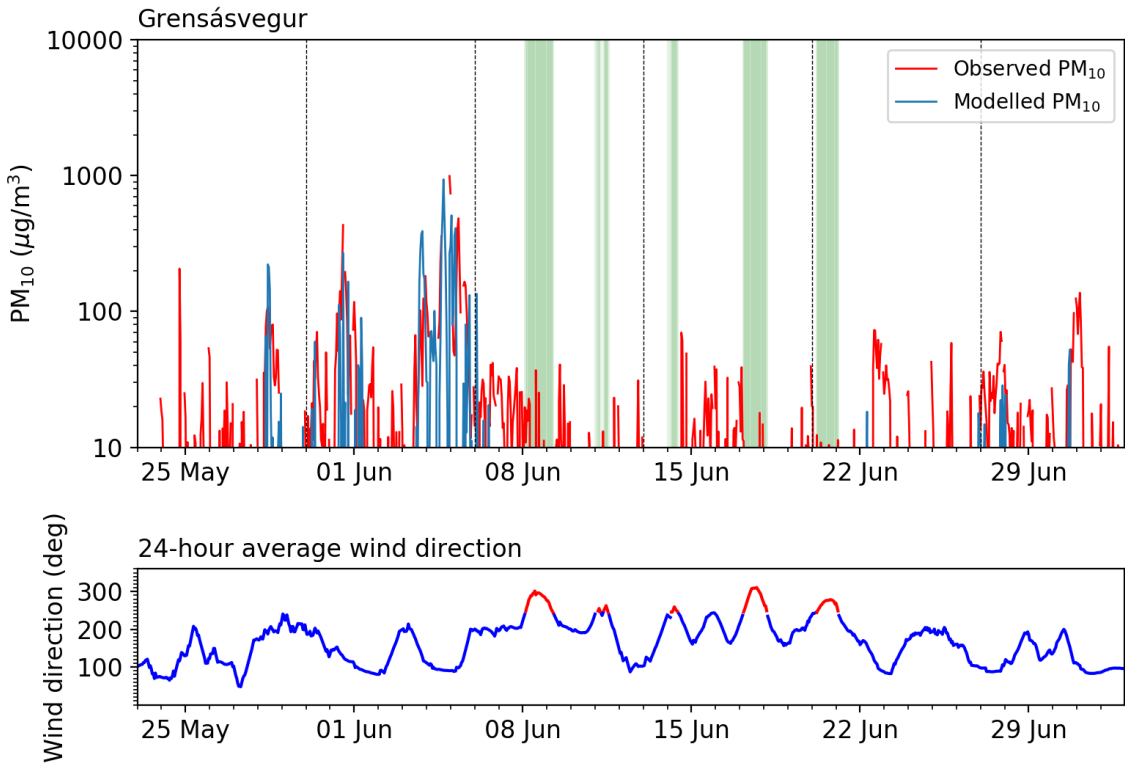


Figure 8 Comparison between observed PM₁₀ concentrations at Grensásvegur (red) and scaled NAME model output (blue) at the same location. Below, a visualization of the 24-hour average direction from which wind was blowing at Tindfjöll shows directions assumed to not be conducive to transporting ash from Eyjafjallajökull to Grensásvegur in red. These same time periods are expressed on the comparison plot with green vertical bars. Dashed vertical lines represent each full week past eruption end.

High PM₁₀ concentration episodes are observed at the Grensásvegur station on 30 May–1 June and 3–6 June (Figure 8). The hit rate at this station is 56.7%, with a 2.0% false alarm rate. Modeled events in the first two weeks following the eruption appear to agree with the observations relatively well again in both timing and relative magnitude. Model predictions do appear again to be truncated in a similar manner to that observed at Heimaland. The small spike on 28 May exhibits this behavior particularly well. This peak, too, ultimately escapes definition as an event, despite instantaneously exceeding 200 µg m⁻³. PM₁₀ concentrations reached a maximum of 1321 µg m⁻³ at on 4 June 2010, in relatively close agreement with the calibrated model output maximum of 939 µg m⁻³ only four hours earlier. Later instances of NAME prediction of smaller amounts of ash remobilization—all peaks visible after 22 June—appear to significantly underestimate both magnitude and duration of measured airborne particulate matter.

Based on the assumptions made regarding the role of wind direction in the provenance of particulate matter observations at Grensásvegur, approximately five distinct time periods between 8–21 June appear to have observed airborne particulate matter with an origin external to the ash source deposit (green bands in Figure 8). This encompassing time period also represents the longest period of time in the weeks immediately following the eruption where NAME predicts no output at Grensásvegur. Nearly every instance of modelled ash resuspension roughly corresponds to a period of time when the average wind direction came

from approximately 90–100°. A notable exception is the brief period representing a short but moderate peak on 28 May, during which the average wind direction very nearly approaches the exclusion zone. Wind directions typically associated with notable NAME predictions are seen nearly a day prior to this spike.

4.3 Data Comparison for the Period September 2010–February 2011

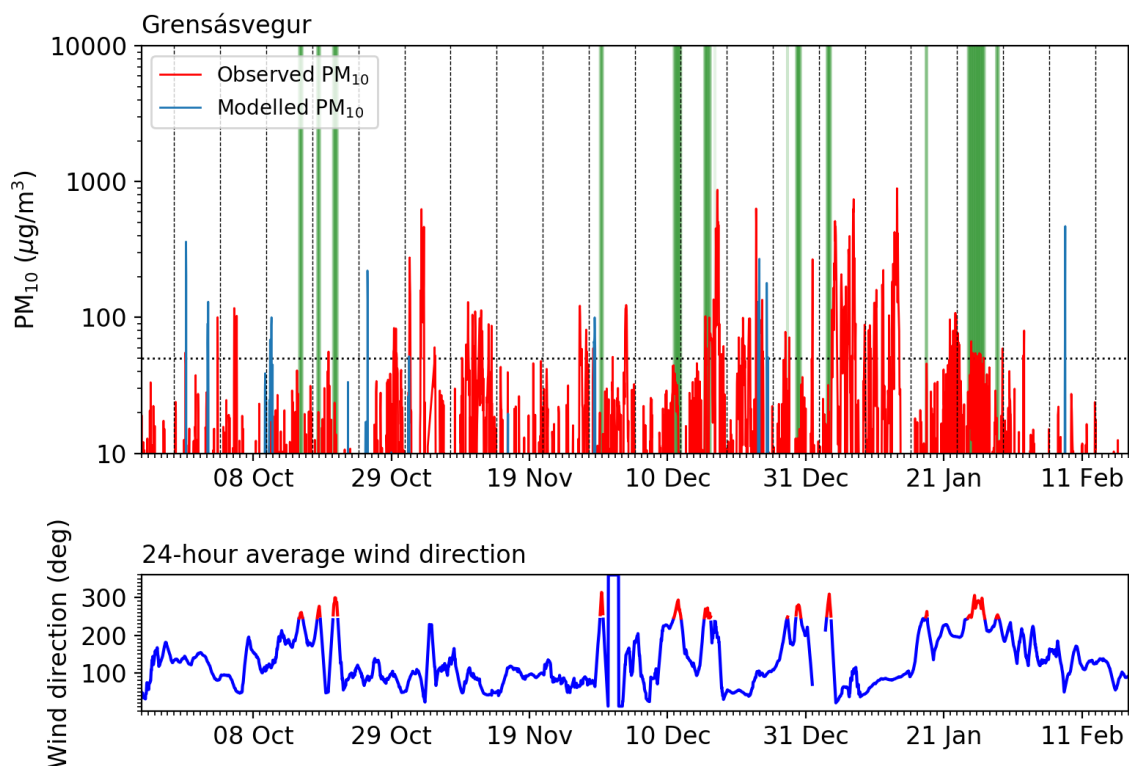


Figure 9 Comparison between observed PM₁₀ concentrations at Grensásvegur (red) and scaled NAME model output (blue) at the same location. Below, a visualization of the 24-hour average direction from which wind was blowing at Tindfjöll shows directions assumed to not be conducive to transporting ash from Eyjafallajökull to Grensásvegur in red. These same time periods are expressed on the comparison plot with green vertical bars. Dashed vertical lines represent each full week past eruption end. A dotted horizontal line at $50 \mu\text{g}/\text{m}^3$ exhibits the PM₁₀ safety threshold.

From 21 September 2010 to 16 February 2011, six distinct periods of average daily PM₁₀ levels in excess of $50 \mu\text{g}/\text{m}^3$ occurred in the observational data at the Grensásvegur station (Figure 9). These observed events took place from 1–3 November, 16–18 December, 22–24 December 2010, 3–4 January 2011, 4–8 January, and 12–14 January. A peak observed concentration of $893 \mu\text{g}/\text{m}^3$ occurred during the last event, on 13 January. Though the NAME model predictions yield a maximum instantaneous peak of $470 \mu\text{g}/\text{m}^3$ on 8 February, none of the visible spikes in the modelled concentrations last long enough in duration to

qualify as an event in terms of the 24-hour rolling averages. As such, there are effectively zero modelled events, yielding both a hit rate and false alarm rate of 0% for Grensásvegur during this time period.

Closeness of fit based on visual inspection is otherwise also low for this time period at this station. Predicted ash resuspension magnitudes are rarely in agreement with those observed. In many cases, primarily those in September–October 2010 and in February 2011, the model drastically overpredicts airborne concentrations with respect to the PM₁₀ observations. This apparent overprediction in these time periods has previously been explained by NAME following precipitation events (Leadbetter et al., 2012). The drying out process of volcanic ash, assumed to cause periods of reduced particle resuspension following large precipitation events, is unaccounted for in the model. The relatively large predicted peak on 25 October seemingly overlying a complete absence of measured concentrations is itself due to a gap in observational data from 22–26 October 2010.

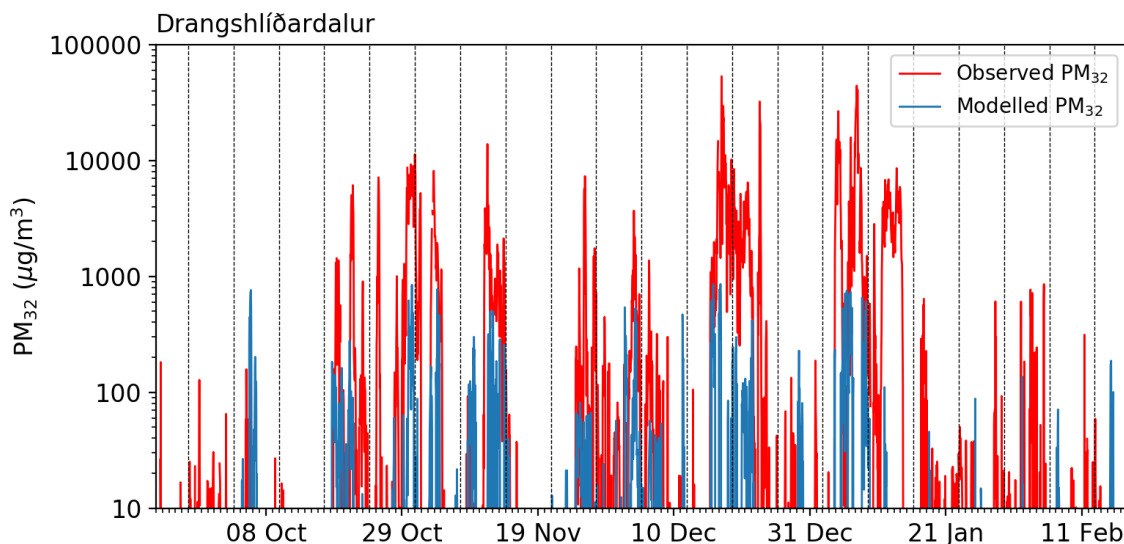


Figure 10 Comparison between observed PM₁₀ concentrations at Drangshlíðardalur (red) and scaled NAME model output (blue) at the same location. Dashed vertical lines represent each full week past eruption end.

For the continuous OPC station at Drangshlíðardalur, located directly within the ash deposit, concentrations of PM₃₂ (particles with a diameter of up to 32 µm) were modelled by NAME to compare to the provided observational data. To calculate hit rate and false alarm rate, the appropriate 24-hour PM₁₀ threshold was scaled up to accommodate the PM₃₂ measurements at this station. Nine event periods were determined: from 20–23 October, 24–26 October, 27 October–4 November, 9–14 November, 24–28 November, 2–7 December, 14–23 December 2010, 3–15 January 2011, and 2–4 February (Figure 10). Though NAME predictions for many of these events approximately capture the timing of peaks, magnitudes are frequently underestimated by many orders. Few events are overestimated, though those that are tend to fall into the previously discussed windows during which precipitation lag (the drying out process of the source) has presumably suppressed observations of ash resuspension. One

notable exception is on 8–9 November when model predictions are nearly three times what was actually observed ($115 \mu\text{g m}^{-3}$ observed on 8 November versus the model output of $300 \mu\text{g m}^{-3}$ on 9 November). At this location, NAME attained only an 18.9% hit rate and 1.6% false alarm rate during the studied time period.

5 Discussion

With the newly derived temporally dependent scaling relationship K_t , the NAME model output appears to agree fairly well with both PM₁₀ monitoring stations at Heimaland and Grensásvegur in the time period immediately following the eruption end. Heimaland hit rate and false alarm rate (71.9% and 2.6%, respectively) are close to the values of 78% and 7% obtained by the previous calibration method (Leadbetter et al., 2012). The systematic lowering of both numbers suggests an overall decrease in NAME output following calibration. This is expected given the systematic decrease of K_t with time under the new scheme.

The original dimensional static coefficient (allowing for direct model output in $\mu\text{g m}^{-3}$) had $K = 1.1 \times 10^7$. If one considers the source file scaling performed prior to the running of NAME, the initial uniform value for ash resuspension was set to 1 g s^{-1} for each source grid rectangle. The rate of emission was scaled in this study to correspond to $1 \text{ g s}^{-1} \text{ km}^{-2}$, yielding an ash resuspension per grid point directly proportional to the surface area of each rectangle. The average area per unit in the sources file is 0.547 km^2 . Scaling the initial calibration coefficient by this amount yields an approximate value of K equivalent to 6.0×10^6 . Given the newly determined temporal relationship, the scaling factor for the first day immediately following an eruption (when $t = 1$) is approximately 5.9×10^6 , in near-perfect agreement with the static scaling value determined by Leadbetter et al. (2012). This time-dependent K_t value decreases by nearly an order of magnitude to 7.8×10^5 by the end of the initial period of study on 2 July 2010, likely contributing to the decrease in hit rate and false alarm rate at Heimaland over that obtained in the initial work regarding resuspension forecasting.

Prior mention is made of the local conditions at the Grensásvegur monitoring station being conducive to higher levels of noise and background events. In addition to the urban location of the monitoring station allowing for potential observation of anthropogenic particle suspension, it lies within a zone of regular deposition of particulate matter from sandy areas and dust plume sources (Arnalds, 2010). Observation data from all of 2009, prior to the fresh deposition of volcanic ash at Eyjafjallajökull, has allowed for the unspoiled view of an annual event history without the influence of readily remobilized volcanic ash. In all of 2009, the daily threshold of average PM₁₀ concentrations above $50 \mu\text{g m}^{-3}$ was exceeded 5.6% of the time (when concurrent 24-hour slices were available for analysis). The previously mentioned maximum event from this time period, $650 \mu\text{g m}^{-3}$ in mid-May 2009, is not far below the maximum peak of $893 \mu\text{g m}^{-3}$ observed in the September 2010–February 2011 window. Only three events from September 2010–February 2011 actually exceeded this 2009 maximum. The average of PM₁₀ concentration from this station during all of 2009 is $21 \mu\text{g m}^{-3}$ (only $14 \mu\text{g m}^{-3}$ from 23 May–2 July 2009), compared to $36 \mu\text{g m}^{-3}$ in the six weeks from 23 May–2 July 2010 immediately following the eruption, and $29 \mu\text{g m}^{-3}$ from September 2010–February 2011. If 2009 is taken as a baseline, and the late spring–early summer period as lying typically below the annual average, it appears evident that the eruption signal introduced by a fresh volcanic ash deposit decreases with time following an initial large spike in the direct wake of an eruption.

In addition to multiple observations of airborne particulate matter at Grensásvegur above the recommended threshold that are unrelated to the ash deposit at Eyjafjallajökull, the OPC station at Drangshlíðardalur sits directly in an area of high aeolian deposition of dust and sand, surrounded on all sides by three points that represent major dust plume areas (Arnalds, 2010).

With this, the apparent calibrated model underestimation of airborne particulate matter concentrations at Drangshlíðardalur and Grensásvegur from September 2010–February 2011 may in fact be a product of natural decay of the ash source deposit. The characteristics of the deposit this far past the end of the eruption appear to contribute still to at least an increase in event strength, but overall annual patterns of non-volcanic ash events may be the cause of this perceived lack of forecast ability. In order to more accurately assess the goodness of fit of NAME utilizing the newly derived scaling relationship K , external dust and sand sources must be accounted for and removed from the observational data.

5.1 Bulk Removal of Glaciers

Following the snowfall in mid-September 2010 that prompted the bulk removal of ash source points overlain by glacial polygons, the appropriateness of performing such a method might be contested, as there is a clear dichotomy in the behavior of large sections of the ash deposit. Satellite imagery in Figure 14 (Appendix B) exhibits the stark contrast in coloration between the pre- and immediately post-eruption Mýrdalsjökull glacier (immediately east of Eyjafjallajökull). In early June, snowfall appears and subsequently melts, again revealing the underlying ash deposit. This gives the first indication of region-specific evolution. It is presumed to be a function of altitude, rather than of deposit thickness, as the thickest deposit is centered on Eyjafjallajökull, rather than on Mýrdalsjökull (Figure 15 in Appendix B). Further inspection of the imagery in Figure 2 shows this same presumed higher-altitude region maintaining its dark coloration, while the surrounding areas appear to have returned to nearly their pre-eruption state.

With the lower altitude regions exhibiting an absence of visible ash deposit only four months following the eruption end, the drastic reduction in K_t value with time receives further supporting evidence. The high-altitude preservation of ash may be indicative of a separate pattern of climatic conditions above a critical altitude: differing precipitation or wind patterns yielding a lower susceptibility to ash remobilization; erosion, compaction, and cementation; and outwash. The contour between the high-altitude area of remaining volcanic ash and the relatively clear surrounding glacial fringe may also very well represent the boundary between zones of ablation and accumulation.

Regardless of the local differences in deposit evolution over the glacial extent, it has been observed that the September 2010 snowfall event that necessitated the permanent removal of source material from the input file remained a permanent effect. The covered ash at the higher altitudes on Mýrdalsjökull never reemerged. With the evidence of visible ash reduction at the lower altitude glacial extents, as well as the drastic reduction in the scaling factor K_t at this point past the eruption end, the bulk manual removal of this source material from the model has been deemed appropriate.

5.2 Applicability to Other Deposits

The ability for this calculated scaling relationship to be applied universally to any volcanic ash deposit in Iceland is uncertain. Given the evidence of differing source evolution behavior under different geographic or climatic circumstances, it is unlikely that an ash deposit of identical composition but in a drastically different physical setting would react in the same manner as the 2010 deposit from Eyjafjallajökull.

A morphological and chemical analysis of freshly deposited ash in Reykjavík following a notable remobilization event in early March 2013 indicated an approximately 50% split in source provenance between the Eyjafjallajökull deposit and ash from the eruption of Grímsvötn (ending in May 2011), with some minor contribution of silicic material from other historical volcanic deposits (Liu et al., 2014). The same study modelled the resuspension event in NAME according to the methods outlined by Leadbetter et al (2012). NAME predictions estimated that the event should have resulted in an ash mixture of 99% Eyjafjallajökull ash and only 1% from Grímsvötn.

In the study by Liu et al. (2014), the areal extent of the Grímsvötn deposit had not yet been published, necessitating prior estimation of source area by modeling the eruption itself. This introduced some uncertainty to the accuracy of the results. It was also assumed in the resulting discussion that the incongruence in observed versus modelled source yield ratios might be due to an evolving scaling factor with time, overestimating the contribution from Eyjafjallajökull in comparison to Grímsvötn. Assuming that the same scaling factor determined in this study could be applied to the Grímsvötn deposit, the expected relative difference in scaling between the two source deposits at a point that far past each eruption results in predictions from Eyjafjallajökull scaled at 99.6% of the amount applied to Grímsvötn. Neglecting the effect of an improperly estimated Grímsvötn source deposit areal extent in the Liu et al. study, applying the newly derived temporal scaling factor independently to each deposit would have little discernible effect on the resulting ash ratios. This is highly suggestive of non-uniform ash deposit evolution for volcanic eruptions in Iceland, due not only to the factors of local geology, geography, and prevailing weather conditions, but also due to characteristics of the individual ash deposits that may govern the ability for remobilization (particle shape and chemical composition, for instance). The vast perceived difference in ash ratios may also, however, point to an overestimation in this study of the rate of decline of K_t following the end of an eruption event.

Testing the applicability of the newly derived K_t to the subsequent Grímsvötn volcanic ash deposit becomes more complicated, due to the prevailing influence of the Eyjafjallajökull source. Future attempts to test the Grímsvötn calibration factor accounting for source evolution with time will need to contend with the removal of this influence. For instance, modeling only the scaled contribution from the Eyjafjallajökull source and subtracting the predictions from observational data to yield particulate matter contributions only from Grímsvötn (and the normal sand and dust resuspension) assumes a perfect model already in place. Any error in this calibration from the 2010 eruption will then only be magnified for subsequent eruption calibrations.

Without calibration on other eruption deposits confirming the uniformity of evolution of Icelandic volcanic ash sources, the ability for this scaling relationship to be applied in the future as a method of hazard prediction in the immediate wake of a volcanic eruption is

uncertain. Anecdotal evidence from the analysis of redeposited ash in Reykjavík in March 2013 suggests the potential for separate eruptions to experience a unique pattern of ash source evolution.

Regardless, if it is assumed that the scaling factor is equally applicable to all volcanic ash in Iceland regardless of its eruption provenance, significant amounts of time have elapsed since the eruption events of Eyjafjallajökull in 2010 and Grímsvötn in 2011 such that the scaling factor applied to each would be approaching the asymptotic value of $K_t(t=\infty) = 6.5 \times 10^5$, roughly an order of magnitude lower than the maximum experienced scaling immediately following the eruption. Based on the magnitude of modelled events at Grensásvegur and Heimaland in May–July 2010, even a ten-fold decrease in model output permits the possibility of events that surpass the $50 \mu\text{g m}^{-3}$ average per day threshold, seeming to underline the necessity of continued daily prediction of ash remobilization over Iceland.

The seasonality of surface conditions must also be investigated. Based on the derived function for K_t , the expected half-life of the ash deposit with respect to its ability to be remobilized is on the order of approximately 2.3 days following the end of an eruption event. Due to this rapid decline in resuspension potential, it is likely that prevailing climatic conditions are at least in part responsible for the rate of evolution of source material. Events that occur in drastically differing seasonal conditions may in fact experience different rates of evolution, yielding an altogether different function for K_t , or otherwise a more highly parameterized function that takes account of the time of year of eruption. A half-life of 2.3 days might appear relatively short in duration, but preliminary work regarding the effect of volcanic eruptions on the frequency of PM suspension events in Iceland has shown that the signal introduced by explosive eruptions is only present for several months following an eruption, if at all (Butwin, von Löwis, Pfeffer, & Thorsteinsson, 2018).

Later analysis of a particularly well-captured resuspension event on 16–17 September 2013, Beckett et al. (2017) determined the scaling factor of the two ash deposits at Eyjafjallajökull and Grímsvötn to be on the order of 1×10^3 . While supporting the conclusion that the ability for ash remobilization decreases with time (and, therefore, as does K), this calculated scaling factor is many times lower than the calculated minimum of this study. This suggests an overestimation of the approached asymptote during calibration in this study, indicating that further decline in scaling factor is expected. Given the initially assumed theoretical decline to a factor of essentially zero as time approaches infinity, the derived relationship for K_t —particularly the location at which the inverse linear regression line passes through the origin—may have the potential to be further refined. Proper handling of the data points causing negative daily K linear relationships would perhaps benefit future analysis, as would the ability to examine the full sets of data from Hvaleyrarholt and Hvolsvöllur using the newly introduced methods of calibration in this study.

6 Summary and Conclusions

Eyjafjallajökull erupted in early 2010, leading to an increase in the frequency of observed PM₁₀ resuspension events in the southern region of Iceland. Airborne particulate matter of this size is known to be harmful to both human health and the agriculture and aviation industries. Modeling of the volcanic ash resuspension dynamics has been implemented at the Icelandic Meteorological Office, and a number of prior limitations have been overcome. The ability to alter the resolution of model input describing the ash deposit areal extent has been accounted for. Additionally, the large-scale seasonal effect of glacial snow cover has been mitigated through manual data removal.

A temporally dependent dimensional scaling factor K_t has been derived through calibration against observed particle suspension data from the time period immediately following the end of the eruption. It allows for direct scaling of NAME output to a PM₁₀ concentration in $\mu\text{g m}^{-3}$. The systematic decrease in K_t with respect to time models the decrease in ability for source ash to be remobilized. This decrease is a product of the evolution of source material, due to various geomorphological and meteorological processes.

The rapid decrease in remobilization as described by the new scaling factor appears to suggest a worsening of the model fit with time. However, in combination with other recent work indicating that the eruption signals of Icelandic volcanoes in the national PM₁₀ observation record are not long in duration, this short-lived dominance of the ash signal may in fact appropriately describe actual conditions. This is further supported by the record of extraneous dust events from the PM₁₀ monitor at Grensásvegur in 2009.

Satellite imagery depicting inhomogeneity in ash deposit evolution—likely a factor of differing geology and geography—underlines the importance of investigating whether this scaling factor is universally applicable to volcanic ash in Iceland. Prior work indicated a vastly different ratio of modeled ash from the 2010 Eyjafjallajökull and 2011 Grímsvötn deposits with respect to an actual sample from a March 2013 remobilization event; this provides further evidence that differences in tephra deposits from explosive eruptions might necessitate calibration on many events.

References

- Arnalds, O. (2010). Dust sources and deposition of aeolian materials in Iceland. *Icelandic Agricultural Sciences*, 23, 3-21.
- Böðvarsdóttir, A. R. (2008). *Mælingar á loftmengandi efnum í Reykjavík 2007 (Measurements of air pollution in Reykjavik 2007)*. Reykjavík: City of Reykjavík.
- Bagnold, R. A. (1941). *The Physics of Blown Sand and Desert Dunes*. New York: Methuen.
- Baxter, P. J., Bonadonna, C., Dupree, R., Hards, V. L., Kohn, S. C., Murphy, M. D., . . . Vickers, B. P. (1999, February 19). Cristobalite in volcanic ash of the Soufrière Hills volcano, Montserrat, British West Indies. *Science*, 283(5405), 1142-1145.
- Beckett, F., Kylling, A., Sigurðardóttir, G., von Löwis, S., & Witham, C. (2017). Quantifying the mass loading of particles in an ash cloud remobilized from tephra deposits on Iceland. *Atmospheric Chemistry and Physics*, 17, 4401-4418.
- Braga, A. L., Zanobetti, A., & Schwartz, J. (2001, November). The lag structure between particulate air pollution and respiratory and cardiovascular deaths in 10 US cities. *Journal of Occupational and Environmental Medicine*, 43(11), 927-933.
- Butwin, M. K., von Löwis, S., Pfeffer, M. A., & Thorsteinsson, T. (2018). The Effects of Volcanic Eruptions on the Frequency of Particulate Matter Suspension Events in Iceland. *Manuscript submitted for publication*, 25.
- Chepil, W. S. (1945). Dynamics of wind erosion: II. Initiation of soil movement. *Soil Science*, 60, 397-411.
- Damby, D. E., Horwell, C. J., Larsen, G., Thordarson, T., Tomatis, M., Fubini, B., & Donaldson, K. (2017). Assessment of the potential respiratory hazard of volcanic ash from future Icelandic eruptions: a study of archived basaltic to rhyolitic ash samples. *Environmental Health*, 16(1), 98.
- Dockery, D. W., Schwartz, J., & Spengler, J. D. (1992, Dec). Air pollution and daily mortality: associations with particulates and acid aerosols. *Environmental Research*, 59(2), 362-373.
- Draxler, R. R., Ginoux, P., & Stein, A. F. (2010). An empirically derived emission algorithm for wind-blown dust. *Journal of Geophysical Research*, 115, D16212.
- European Parliament and Council. (2008, June 11). Directive 2008/50/EC of the European Parliament and of the Council of 21 May 2008 on ambient air quality and cleaner air for Europe. *Official Journal of the European Union*, 152, 1-44.

- Fécan, F., Marticorena, B., & Bergametti, G. (1998, December). Parameterization of the increase of the aeolian erosion threshold wind friction velocity due to soil moisture for arid and semi-arid areas. *Annales Geophysicae*, 17(1), 149-157.
- Folch, A., Mingari, L., Osores, M. S., & Collini, E. (2014). Modeling volcanic ash resuspension – application to the 14–18 October 2011 outbreak episode in central Patagonia, Argentina. *Natural Hazards and Earth System Sciences*, 14, 119-133.
- Forbes, L., Jarvis, D., Potts, J., & Baxter, P. J. (2003, March). Volcanic ash and respiratory symptoms in children on the island of Montserrat, British West Indies. *Occupational and Environmental Medicine*, 60(3), 207-211.
- Gellert, W., Gottwald, S., Hellwich, W., Kästner, H., & Künstner, H. (1989). The Spherical Triangle. In W. Gellert, S. Gottwald, W. Hellwich, H. Kästner, H. Künstner, W. Gellert, S. Gottwald, W. Hellwich, H. Kästner, & H. Künstner (Eds.), *VNR Concise Encyclopedia of Mathematics (Second Edition)* (2nd Edition ed., pp. 262-272). New York: Van Nostrand Reinhold.
- Gilette, D. A., Adams, J., Muhs, D., & Kihl, R. (1982, October 20). Threshold friction velocities and rupture moduli for crusted desert soils for the input of soil particles into the air. *Journal of Geophysical Research*, 87, 9003-9015.
- Gislason, S. R., Hassenkam, T., Nedel, S., Bovet, N., Eiriksdottir, E. S., Alfredsson, H. A., ... Stipp, S. L. (2011). Characterization of Eyjafjallajökull volcanic ash particles and a protocol for rapid risk assessment. *Proceedings of the National Academy of Sciences of the United States of America*, 108(18), 7307-7312.
- Gudmundsson, M. T., Thordarson, T., Höskuldsson, Á., Larsen, G., Björnsson, H., Prata, F. J., ... Jónsdóttir, I. (2012). Ash generation and distribution from the April-May 2010 eruption of Eyjafjallajökull, Iceland. *Scientific Reports*, 2, 12.
- Hadley, D., Hufford, G. L., & Simpson, J. J. (2003, October). Resuspension of Relic Volcanic Ash and Dust from Katmai: Still an Aviation Hazard. *Weather and Forecasting*, 19, 829-840.
- Icelandic Meteorological Office. (2012). *The 2010 Eyjafjallajökull eruption, Iceland*. Montréal: International Volcanic Ash Task Force (IVATF).
- Jones, A. R., Thomson, D. J., Hort, M., & Devenish, B. (2007). The U.K. Met Office's next-generation atmospheric dispersion model, NAME III. In C. Borrego, & A. L. Norman (Ed.), *Air Pollution Modeling and Its Application XVII (Proceedings of the 27th NATO/CCMS International Technical Meeting on Air Pollution Modelling and its Application)* (pp. 580-589). New York: Springer.
- Leadbetter, S. J., Hort, M. C., von Löwis, S., Weber, K., & Witham, C. S. (2012). Modeling the resuspension of ash deposited during the eruption of Eyjafjallajökull in spring 2010. *Journal of Geophysical Research*, 117.

- Liu, E. J., Cashman, K. V., Beckett, F. M., Witham, C. S., Leadbetter, S. J., Hort, M. C., & Guðmundsson, S. (2014). Ash mists and brown snow: Remobilization of volcanic ash from recent Icelandic eruptions. *Journal of Geophysical Research: Atmospheres*, *119*, 9463-9480.
- Marticorena, B., & Bergametti, G. (1995). Modeling the atmospheric dust cycle: 1 Design of a soil-derived dust emission scheme. *Journal of Geophysical Research*, *100*(D8), 16415-16430.
- Met Office. (2014). *Iris 2.1: A powerful, format-agnostic, and community-driven Python library for analysing and visualising Earth science data*. Retrieved October 2018, from Iris 2.1.0 documentation: <https://scitools.org.uk/iris/docs/latest/index.html>
- Moritz, H. (2000). Geodetic Reference System 1980. *Journal of Geodesy*, *74*(1), 128-133.
- Searl, A., Nicholl, A., & Baxter, P. J. (2002, August). Assessment of the exposure of islanders to ash from the Soufriere Hills volcano, Montserrat, British West Indies. *Occupational and Environmental Medicine*, *59*(8), 523-531.
- Sigurdsson, O. (2005). GLIMS Glacier Database. Boulder, CO.
- Stephenson, D. B. (2000, April). Use of the “Odds Ratio” for Diagnosing Forecast Skill. *Weather and Forecasting*, *15*(2), 221-232.
- Thorsteinsson, T., Gísladottir, G., Bullard, J., & McTainsh, G. (2011). Dust storm contributions to airborne particulate matter in Reykjavík, Iceland. *Atmospheric Environment*, *45*, 5924-5933.
- Thorsteinsson, T., Jóhannsson, T., Stohl, A., & Kristiansen, N. I. (2012, January 10). High levels of particulate matter in Iceland due to direct ash emissions by the Eyjafjallajökull eruption and resuspension of deposited ash. *Journal of Geophysical Research*, *117*(B9), B00C05.
- Veness, C. (2017). *Calculate distance, bearing and more between Latitude/Longitude points*. Retrieved January 24, 2018, from <https://www.movable-type.co.uk/scripts/latlong.html>
- Wilson, T. M., Cole, J. W., Stewart, C., Cronin, S. J., & Johnston, D. M. (2011, April). Ash storms: impacts of wind-remobilised volcanic ash on rural communities and agriculture following the 1991 Hudson eruption, southern Patagonia, Chile. *Bulletin of Volcanology*, *73*(3), 223-239.

Appendix A: Technical Aspects

A.1 Setup of Modeling Environment at IMO

Prior to the commencement of this ash resuspension modelling at the IMO using NAME, it had been decided to install the most recent release of the modelling environment—NAME version 7.1—for the purposes of this project. Due to the gridded binary (GRIB) nature of the numerical weather prediction (NWP) data to be employed as input files in the model runs, consultation with individuals at the UK Met Office with expertise in the usage of NAME revealed that endeavoring to upgrade to the latest release required that the NAME executable be compiled locally. This source code compilation required a run-time dynamic linking to the local GRIB Application Programming Interface (API) library. Obstacles involving both file access permissions on the working machine at this time and the lack of a required compiler necessitated that the working environment be migrated to a separate machine, one at that point being used solely for operational purposes at the IMO. NAME v7.1 was, after a period of troubleshooting aided by the UK Met Office, successfully compiled on this new machine. This migration ultimately led to the benefit of faster model run times due to increased processing power on the destination machine.

Having been supplied with existing versions of input files *input.txt* and *sources.txt* (see Appendix D) by Frances Beckett in a personal communication on 2 October 2017, a period of trial and error in providing the proper formatting and meteorological data definitions was required to allow for the execution of NAME using the GRIB files from the European Centre for Medium-Range Weather Forecasts (ECMWF) as the driving meteorology. Descriptions of the function of each of these input files are included in Appendix D.

On the machine with the successfully compiled and operational NAME v7.1 executable file, a number of scripts were written to automate tasks that would be regularly repeated throughout the course of performing model runs. One Python script accepted zero, one, or two input arguments—in *yyyymmdd* string format—and modified both the emission times in the input file *sources.txt* and the model start and end times in *input.txt* accordingly (no modification if given no arguments, a change in start time with a standard duration given one argument, or an overridden emission and model run time if given two input dates).

The same script then called the NAME executable with the appropriate input files as command line arguments, initializing a model run. A second shell script was written that called this first script, managed the renaming of the output file containing the meteorological data (so as to prevent overwriting previous output on subsequent model runs), and synced the newly created output files to the separate machine that handled the visual postprocessing of data.

A workspace on the original working machine was maintained due to the presence of a previously installed Python library called Iris that facilitates the visualization of data (Met Office, 2014). On this machine, a number of scripts in various scripting languages were

produced that offered a variety of functions operating on a single string input representing a given date in the format *yyyymmdd*. One Python script extracted the meteorological output from NAME at a predefined point—Tindfjöll (at 63.7757°N, 19.6773°W), based on a preexisting meteorological output point in the input file supplied by the UK Met Office—and output a three-plot figure depicting the 24 hours of wind speed (m s^{-1}), wind direction (degrees), and wind friction velocity u^* (m s^{-1}) at this location. A second script did the same, but for only a single plot of the 24 hours of precipitation (mm h^{-1}) at the same location. A third script, originally written and supplied by Frances Beckett of the UK Met Office, was modified for use at the IMO for plotting a map of resuspended ash air concentrations over all of Iceland as an average over the boundary layer depth. A shell script was written that took in the date string in *yyyymmdd* format and subsequently ran all three of the above scripts for the requested given day, outputting the results as PNG files.

For much of the duration of the modelling research process, hard disk space constraints on the machine handling the modelling necessitated that long-term modelling processes (i.e.: the modelling of events from 2010–2011) be paused at regular intervals to facilitate the swapping of NWP GRIB files. The equivalent to five days of NWP data were able to fit at one time in the location from which such files were read by NAME. In the course of processing unbroken periods of many months’ duration, old files would require deletion and replacement by those to be next used in the processing. This space constraint was later rectified by the IMO, allowing for the full extent of a model period to be processed at once.

A.2 Retrieval of Past NWP Data

Past numerical weather prediction data from ECMWF was required from the periods of 23 May–3 July 2010 and 21 September 2010–17 February 2011 for the purposes of running NAME for the times during which air quality observation data was available. A shell script already in use at the IMO was modified to download each day of data from these periods in the appropriate format and containing the required parameters. Due to physical space constraints, it was only possible to request three days of data at one time, which varied in total download time from 45 minutes to upwards of many hours, depending on nature of the concurrent workload manager queue during download of these data. On occasion, downloaded files would be fragmented or missing altogether, requiring deletion and re-download of certain three-hour duration GRIB files. This initial period of data accumulation took several weeks.

The following sequence was performed for each set of three days of data: Connect to the ECMWF workspace through Secure Shell (SSH), requiring a secure numerical password generated via a key generator and PIN; run the shell script for each day in the set to be queued for download; wait for data download to complete; connect again to the ECMWF workspace through File Transfer Protocol (FTP) to transfer downloaded files to the local machine; delete the downloaded data to free up disk space.

Following the discussion central to the following section and the requirement for NWP files with previously unrequired fields, it became necessary to perform this data retrieval once more, covering the entire extent of the period of study.

A.3 Preprocessing of NWP Data

Regular observation of the meteorological output visual plots from Tindfjöll illustrated that what was assumed to be a precipitation rate (in mm h^{-1}) appeared to be accumulating throughout the course of each day, and resetting to zero at midnight (00:00). Consultation with Frances Beckett and Andrew Jones of the UK Met Office revealed that this was in fact due to the nature of ECMWF NWP data containing no standard field equating to a precipitation rate; rather, it contains only fields for total accumulation. In the case of occasional use of this NWP data by the UK Met Office, it required preprocessing to convert accumulation to hourly rate.

The preprocessing module had been developed to be used for files of a specific content format and naming convention, to which the data employed in this study were incompatible. Initially, the source code of specific modules (written in Fortran 90) were edited for use by the IMO according to the format of the files to be used. However, due to the nature of the extended time period covered by this project, an issue arose that required further attention.

The preprocessing module itself operated on the basic assumption that as precipitation accumulated over the extent of a file (or batch of files corresponding to a longer duration), the fields representing this accumulation could be read in, and the total accumulation from the previous time slice subtracted from the current amount, yielding a precipitation rate between the two times. However, the duration of this study covered such a period of time that a sequence of files representing a continuous period of precipitation accumulation was unable to be accommodated. Thus, during the retrieval of data, the files were obtained such that each day at midnight represented a period of renewed accumulation of precipitation, beginning at a value of 0 mm in the file representing midnight (00:00) on that day. A new method was required to handle the case at midnight of each day, where subtracting the accumulation from the previous day would otherwise result in a negative rate of precipitation. Additionally, as each day started anew with an accumulation of 0 mm, there was no indication of how to derive a rate at midnight.

A lack of experience writing code in Fortran necessitated that the core mechanics required to process the NWP files in use by the IMO be rebuilt in Python. The coding logic behind the primary modules was parsed and recreated line for line, following only the branches of logic necessary for the specific files to be processed (and thus ignoring the robustness of the original module for dealing with file structures of varying format), using the Python *grib_api* module.

To handle the case at midnight where no historical data was available, the newly built Python preprocessor would temporarily maintain the precipitation rates at 21:00 each day (given that time steps were in 3-hour increments from the 2010–2011 ECMWF data). It would then jump forward to 03:00 the following day, and calculate the precipitation rate following 00:00 of that day. With the rates for 03:00 and the 21:00 of the previous day, the rate of precipitation at time 00:00 was roughly estimated as being the average between these two rates.

It is acknowledged that this method may not accurately describe the meteorological conditions at that time. However, given the nature of the input files, it was deemed the most appropriate way to otherwise accommodate the lack of appropriate fields.

Appendix B: Supplementary Figures

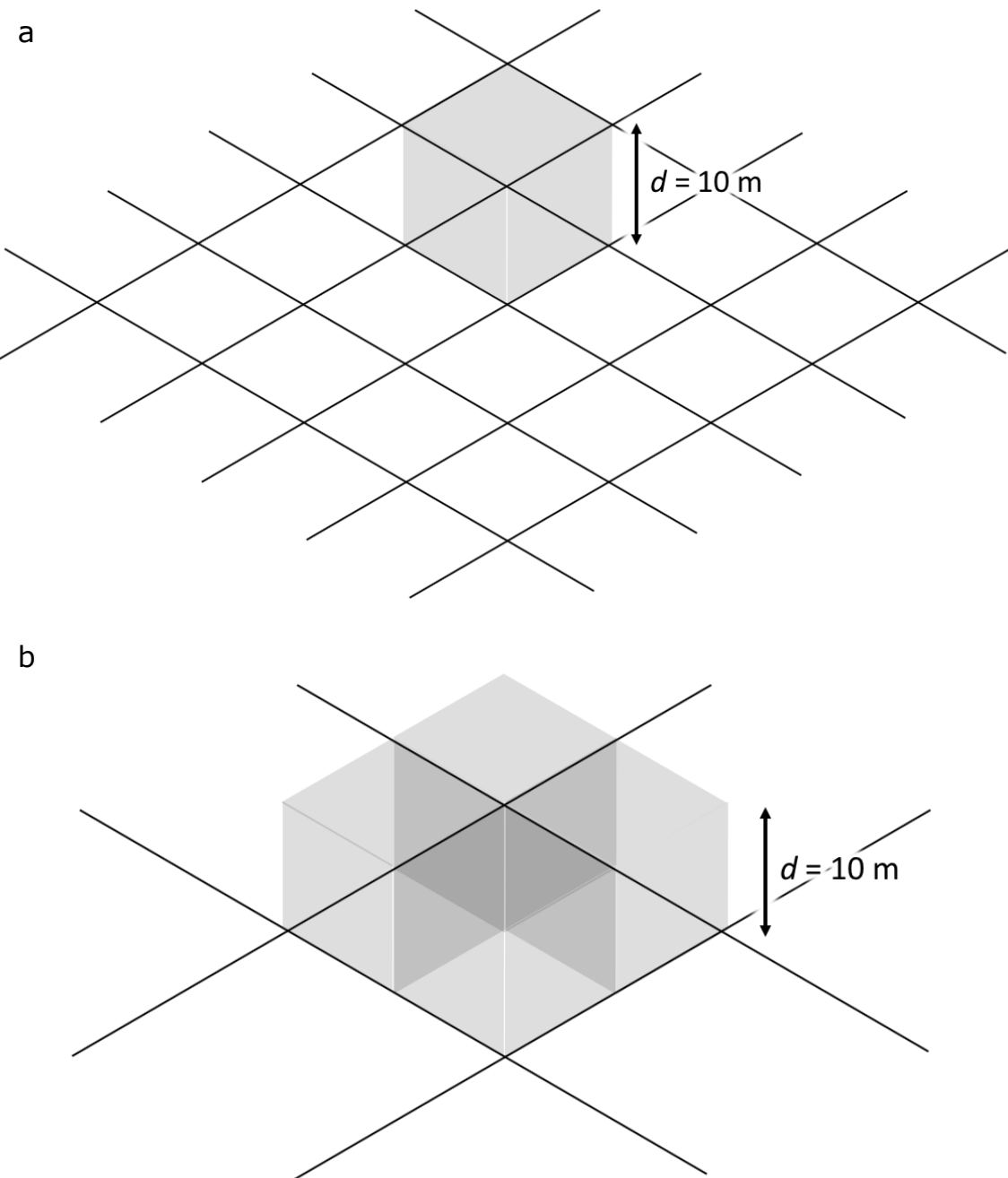


Figure 11 Schematic showing the effect of a change in source grid resolution. The bottom image (b) represents a grid where the edge size has doubled compared to that on the top (a), resulting in a particle release volume of four times the initial volume. In this scheme, NAME releases particles uniformly above the release area to a depth of 10 m.

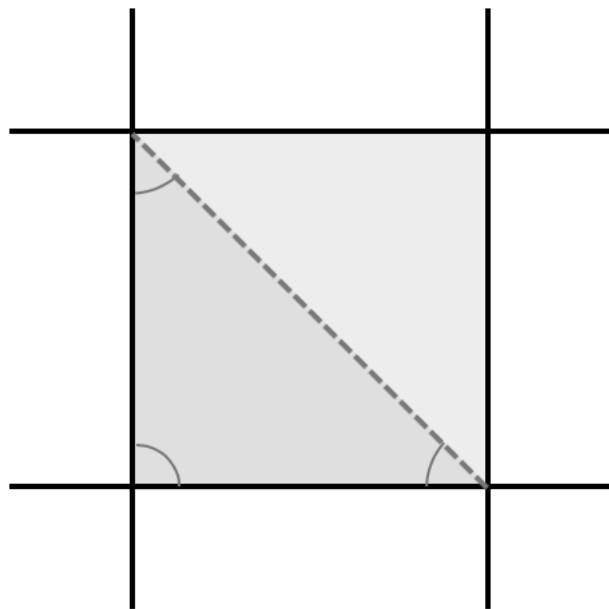


Figure 12 Schematic showing the division of a source grid cell into a triangle for the purposes of calculating surface area. Surface calculations were performed for each triangular half of the cell and were summed.

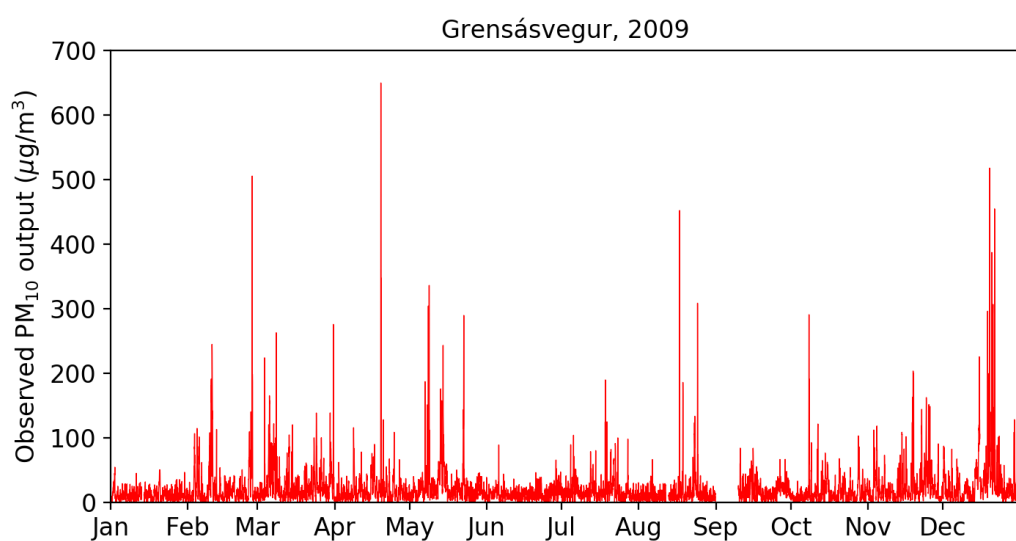


Figure 13 PM_{10} measurements at Grensásvegur for all of 2009.

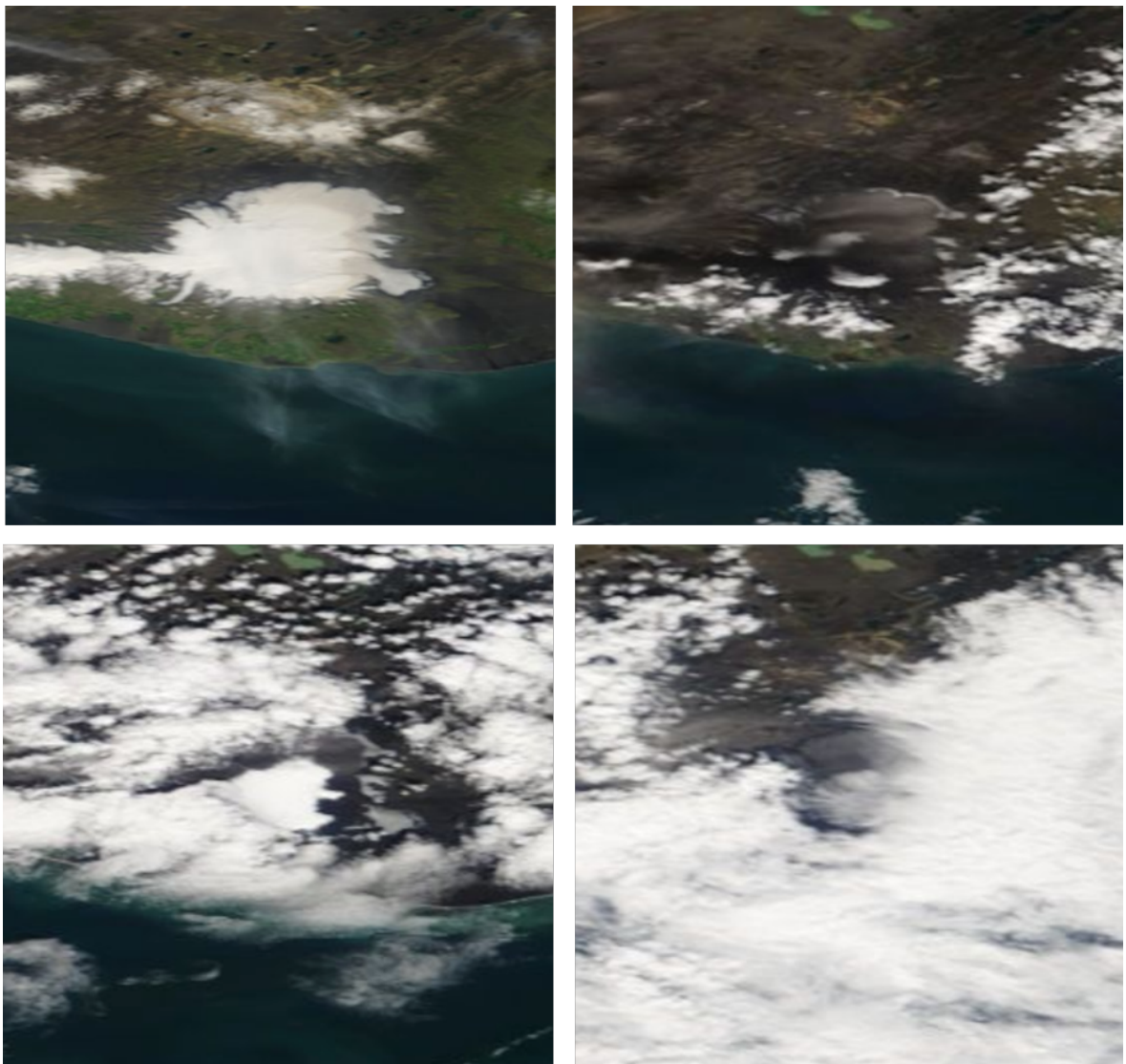


Figure 14 MODIS true color satellite imagery over Eyjafjallajökull glacier on 9 July 2009 (top left), 25 May 2010 (top right), 2 June 2010 (bottom left), and 7 June 2010 (bottom right). The image from 2009 shows a relatively clear shot of the glacier prior to deposition of volcanic ash. The series from May–June in the remaining three images shows not only the relatively full coverage of the glacier in volcanic ash, but also the appearance and subsequent disappearance of snow over the area in the central region of the glacier, presumably above a particular altitude.

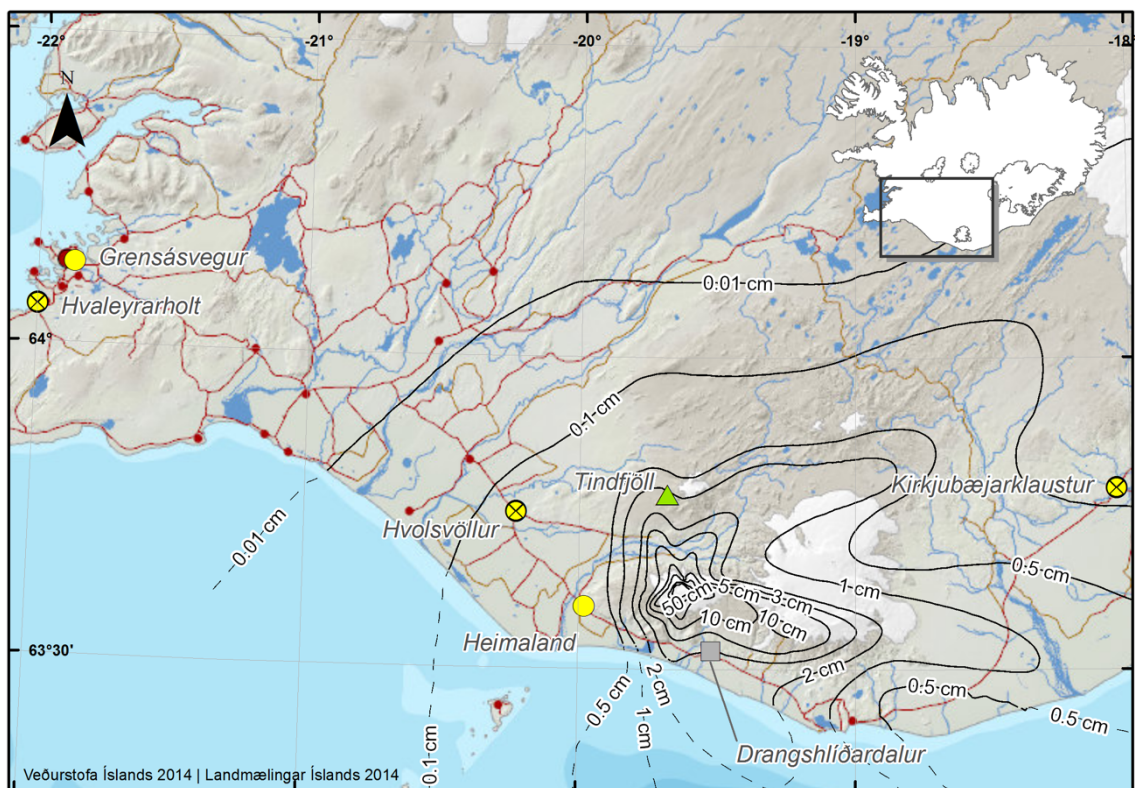


Figure 15 Map showing the isopach thickness of the Eyjafjallajökull tephra deposit (Gudmundsson et al., 2012).

Appendix C: Utilized Scripts

No accommodation has been made for the wrapping of text in the following lines of code that occurs due to the presence of lines that exceed the recommended maximum length.

C.1 *scale_release.py*

This Python script takes in a single filename as an argument: the file on which the scaling of resuspended ash to account for areal extent is to be performed. Its function is described in the above sections. The end result is a separate output file otherwise identical to the first, but with the filename suffix ‘_scaled’ and the initial source strength ‘RESUSPENDED_ASH 1 g/s’ modified to represent 1 g s⁻¹ per rectangular grid area.

```
#!/usr/bin/env/python

import sys
import csv
import os
import math

# Average radius, from
# https://link.springer.com/article/10.1007%2Fs001900050278
rho = 6371.0088

def toRadians(degrees):
    return degrees*2.*math.pi/360.

def toDegrees(radians):
    return (radians*360./(2.*math.pi)+360.)%360.

def constrainQuadrants(theta1,theta2):
    if abs(theta1-theta2) > 180:
        theta1 = (theta1+180.)%360.
        theta2 = (theta2+180.)%360.
    return theta1,theta2

# Here, phi represents latitude, and lam (lambda) longitude
def angleCalc(point1,point2,point3):
    phi1 = toRadians(point1[1])
    lam1 = toRadians(point1[0])
    phi2 = toRadians(point2[1])
    lam2 = toRadians(point2[0])
    phi3 = toRadians(point3[1])
    lam3 = toRadians(point3[0])
    # Bearing from point2 to point1
    theta1 = toDegrees(math.atan2(math.sin(lam1-lam2)*math.cos(phi1), \
        math.cos(phi2)*math.sin(phi1)-math.sin(phi2)*math.cos(phi1)* \
        math.cos(lam1-lam2)))
    # Bearing from point2 to point3
    theta2 = toDegrees(math.atan2(math.sin(lam3-lam2)*math.cos(phi3), \
        math.cos(phi2)*math.sin(phi3)-math.sin(phi2)*math.cos(phi3)* \
        math.cos(lam3-lam2)))
    theta1,theta2 = constrainQuadrants(theta1,theta2)
    values = [theta1,theta2]
    return toRadians(abs(max(values)-min(values)))
```

```

def findAngles(u,v,w):
    return anglecalc(v,w,u),anglecalc(u,v,w),anglecalc(w,u,v)

def triangleArea(u,v,w):
    a,b,c = findAngles(u,v,w)
    return (a+b+c-math.pi)*rho**2

# Returns area of grid square in km^2
def area(x,y):
    if x < 0: # Convert longitude to deg. E
        x += 360.
    # Find four corners
    topL = (x-0.005,y+0.005)
    topR = (x+0.005,y+0.005)
    botL = (x-0.005,y-0.005)
    botR = (x+0.005,y-0.005)
    return
sum([triangleArea(topL,botR,botL),triangleArea(topL,topR,botR)]) 

# Pads the header with proper whitespace
def pad(filename,index):
    with open(filename,'rb') as f, open('temp','wb') as g:
        reader = csv.reader(f)
        writer = csv.writer(g)
        # Write first header:
        writer.writerow(next(reader))
        header = next(reader)
        data = next(reader)
        header[index] = header[index].strip().rjust(len(data[index]))
        writer.writerow(header)
        writer.writerow(data)
        for line in reader:
            writer.writerow(line)
        os.rename('temp',filename)

def main(*args):
    filename = args[0][0]
    newfile = filename.split('.')[0] + '_scaled.' + filename.split('.')[1]
    with open(filename,'rb') as f, open('temp','wb') as g:
        reader = csv.reader(f)
        writer = csv.writer(g)
        # Write first header:
        writer.writerow(next(reader))
        # Find indices of longitude (X), latitude (Y), Source Strength
        header = next(reader)
        for item in header:
            if item.strip() == 'X':
                lon = header.index(item)
            if item.strip() == 'Y':
                lat = header.index(item)
            if item.strip() == 'Source Strength':
                strength = header.index(item)
        writer.writerow(header)
        for line in reader:
            A = area(float(line[lon]),float(line[lat]))
            source = line[strength].split()
            source[1] = str(A)
            line[strength] = ' '+ '+' .join(source)
            writer.writerow(line)
    os.rename('temp',newfile)
    pad(newfile,strength)

if __name__ == "__main__":
    if len(sys.argv) > 1:
        main(sys.argv[1:])
    else:
        print "Please provide one input file as an argument!"

```

C.2 *calibration_plot_only.py*

This Python script takes in integer arguments between 1 and 6 that correspond to predetermined station data. The numerical arguments refer to all six original stations from which data was obtained, in alphabetical order; additional functionality that would allow for inclusion of the data from Grensásvegur, from September 2010–February 2011, has been commented out but retained.

For each argued location (which may be stacked concurrently in any combination), an object was created that would store both time and concentration values from observation data and NAME output. For each location, background PM levels were calculated by iteration (see method explanation in Section 3.3.1).

The exception to this is the station at Drangshlíðardalur; due to its proximity directly within the volcanic ash deposit, data noise was so prevalent as to exclude the iterative method from possible proper function. Such high level of variation caused apparent over-iteration and resulted in significantly lower background levels than determined reasonable. As such, the original plan called for adoption of the values for background mean and standard deviation from the nearest station (Heimaland). The previously determined values were hard-coded, to allow for proper code execution in instances when calculations and plotting were called for at Drangshlíðardalur but not at Heimaland. However, it was realized that incompatibility between measurements (PM_{10} at Heimaland versus PM_{32} at Drangshlíðardalur) precluded this basic substitution as a possibility. The code allowing for this substitution at Drangshlíðardalur remains, despite its lack of use.

Additional unused functionality remains.

```
#!/usr/bin/env python
# -*- coding: utf-8 -*-
import csv
import matplotlib.pyplot as plt
import datetime as dt
from matplotlib.ticker import FormatStrFormatter
import sys
import numpy as np
from scipy.stats import linregress
from scipy.optimize import curve_fit
import math

def main(*args):

    class Location(object):
        def __init__(self, location):
            self.location = location
            self.nametimes = None
            self.namedata = None
            self.obstimes = None
            self.obsdata = None

    locations = [
        'Drangshlidardalur',
        'Grensasvegur',
        'Heimaland',
        'Hvaleyrarholt',
        'Hvolsvollur',
        'Kirkjubaejklaustur'
    ]
```

```

# Selects locations based on input arguments:
if len(args[0]) > 0:
    temp = [locations[int(i)-1] for i in args[0]]
    locations = temp

# local file locations
namedir =
'/Users/Cameron/Desktop/Masters_Project/Aug10/NAME_output/'
obsdir =
'/Users/Cameron/Desktop/Masters_Project/Aug10/Observed_output/'

# Sets up dict data structure containing all data ( observed and modelled)
datadict = {}

# For each location based on input arguments...
for location in locations:
    # create object that contains datetimes and data, observed and modelled
    obj = Location(location)
    times = []
    data = []
    with open(obsdir+'Observed_'+location+'.csv', 'rb') as f:
        reader = csv.reader(f)
        for line in reader:
            #times.append(line[0])
            if location != 'Drangshlidardalur':
                times.append(dt.datetime.strptime(line[0], '%Y-%m-%d %H:%M:%S'))
            else:

                times.append(dt.datetime.strptime(line[0], '%m/%d/%y %H:%M'))
                data.append(line[1])
            # if location == 'Grensasvegur':
            #     with open(obsdir+'Observed_'+location+'_2.csv') as f:
            #         reader = csv.reader(f)
            #         next(reader) # Strip header
            #         for line in reader:
            #             try:
            #                 float(line[1])
            #             #
            times.append(dt.datetime.strptime(line[0], '%Y-%m-%d %H:%M'))
            #                 data.append(line[1])
            #             except ValueError:
            #                 pass
    obj.obstimes = times
    obj.obsdata = data
    # Use the Drangshlidardalur data with the glaciers removed
    if location == 'Drangshlidardalur':
        times = []
        data = []
        with open(namedir+'NAME_'+location+'_removal.csv', 'rb') as f:
            reader = csv.reader(f)
            for line in reader:
                #times.append(line[0])
                times.append(dt.datetime.strptime(line[0], '%Y-%m-%d %H:%M:%S'))
                data.append(line[1])
        obj.nametimes = times
        obj.namedata = data
        datadict[location] = obj
    else:
        times = []
        data = []
        with open(namedir+'NAME_'+location+'.csv', 'rb') as f:
            reader = csv.reader(f)
            for line in reader:

```

```

        #times.append(line[0])
        times.append(dt.datetime.strptime(line[0], '%Y-%m-
%d %H:%M:%S'))
    data.append(line[1])
    # if location == 'Grensasvegur':
    #     with open(namedir+'NAME_'+location+'_2.csv', 'rb') as
f:
    #         reader = csv.reader(f)
    #         for line in reader:
    #             try:
    #                 float(line[1])
    #
    times.append(dt.datetime.strptime(line[0], '%Y-%m-%d %H:%M:%S'))
    #                     data.append(line[1])
    #                     except ValueError:
    #                         pass
    obj.nametimes = times
    obj.namedata = data
    datadict[location] = obj

# Create dict holding lists of all OBSERVED data points, for later
# calculation of background averages
avglists = {}

for location in datadict:
    obj = datadict[location]
    temparray = []
    for i in range(len(obj.obstimes)):
        if not obj.obsdata[i].lower() == 'nan':
            temparray.append(float(obj.obsdata[i]))
    avglists[location] = temparray

nlimit = 3
total_days = 270
binlength = 1
observed = {}
modelled = {}
colors = {}
# Number of time bins following the eruption
for i in range(int(math.ceil(float(total_days)/float(binlength)))):
    observed[i] = []
    modelled[i] = []
    colors[i] = 'k'

locationcolors = {
    'Drangshlidardalur':'g',
    'Grensasvegur':'k',
    'Heimaland':'r',
    'Hvaleyrrarholt':'b',
    'Hvolsvollur':'c',
    'Kirkjubaejklaustur':'y'
}
t0 = dt.datetime(2010,05,23)

# The entirety of the data
whole_obs = []
whole_mod = []

# For splitting up plotting by location
observedbylocation = {}
modelledbylocation = {}
for location in locations:
    observedbylocation[location] = [ [] for i in
range(int(math.ceil(float(total_days)/float(binlength)))) ]
    modelledbylocation[location] = [ [] for i in
range(int(math.ceil(float(total_days)/float(binlength)))) ]
    markers = {
        'Drangshlidardalur': '>',

```

```

    'Grensasvegur': 'o',
    'Heimaland': '^',
    'Hvaleyrarholt': 's',
    'Hvolsvollur': 'x',
    'Kirkjubaejklaustur': 'D'
}

# Calculate background PM values for each location, through
iteration
# (MAY NOT BE APPROPRIATE!)
for location in locations:

    # Uses Heimaland background due to close proximity
    if location == 'Drangshlidardalur':
        avg = 10.856747
        stdev = 3.859567

    else:
        avg = np.mean(avglists[location])
        stdev = np.std(avglists[location])

        while avg+2*stdev < max(avglists[location]):
            avglists[location] = [value for value in
avglists[location] if value < avg+2.*stdev]
            avg = np.mean(avglists[location])
            stdev = np.std(avglists[location])

    print 'Average background PM10 at %s: %f microns/m^3, st.dev.: %f' % \
          (location,avg,stdev)

    obj = datadict[location]

    with open('Observed_and_modelled_'+location+'.csv','wb') as f:
        writer = csv.writer(f)
        writer.writerow(['Datetime','Observed','Modelled'])

        for time in datadict[location].obstimes:
            d_t = time-t0
            week = d_t.days//binlength

            try:
                if float(obj.obsdata[obj.obstimes.index(time)]) - (stdev*2.) > avg and float(obj.namedata[obj.nametimes.index(time)]) > 0:
                    observed[week].append(float(obj.obsdata[obj.obstimes.index(time)]) - avg)
                    modelled[week].append(float(obj.namedata[obj.nametimes.index(time)]))
            except:
                whole_obs.append(float(obj.obsdata[obj.obstimes.index(time)]) - avg)
                whole_mod.append(float(obj.namedata[obj.nametimes.index(time)]))

        observedbylocation[location][week].append(float(obj.obsdata[obj.obstimes.index(time)]) - avg)
        modelledbylocation[location][week].append(float(obj.namedata[obj.nametimes.index(time)]))

    writer.writerow([t_n,float(obj.obsdata[obj.obstimes.index(time)]) - avg, float(obj.namedata[obj.nametimes.index(time)])])

    writer.writerow([time,float(obj.obsdata[obj.obstimes.index(time)]) - avg, float(obj.namedata[obj.nametimes.index(time)])])

```

```

        except ValueError:
            pass

    # Calculate slope and intercept of line for ALL data (as done in
    Leadbetter et al.)
    slope,intercept,r,_,_ = linregress(whole_mod,whole_obs)

    print 'y = %fx + %f' % (slope,intercept)
    x = [0,0.02]
    y = [f*slope+intercept for f in x]

    k = {}
    weight = {}
    for location in locations:
        k[location] = [ [] for i in
range(int(math.ceil(float(total_days)/float(binlength)))) ]
        weight[location] = [ [] for i in
range(int(math.ceil(float(total_days)/float(binlength)))) ]

    # Dimensions of box to zoom in on for plot 2
    zoomx = 0.003
    zoomy = 3000

    # Set up figure for plotting
    # fig,ax1 = plt.subplots(1, figsize=(14,6))
    fig,ax1 = plt.subplots(1, figsize=(8,4))
    # plt.rcParams['mathtext.fontset'] = 'cm'
    # fig,(ax1,ax2) =
    plt.subplots(2,figsize=(14,8),gridspec_kw={'height_ratios':[4,1]})
    # ax2.plot([0,39],[0,0],'k--',lw=0.5)
    # ax2.set_xlim([0,39])
    numberofpoints = 0

    hexcolors = [
        '#FF0A00',
        '#F80906',
        '#F2090D',
        '#EC0914',
        '#E6081A',
        '#DF0821',
        '#D90828',
        '#D3082E',
        '#CD0735',
        '#C7073C',
        '#C00743',
        '#BA0749',
        '#B40650',
        '#AE0657',
        '#A8065D',
        '#A10664',
        '#9B056B',
        '#950572',
        '#8F0578',
        '#89057F',
        '#820486',
        '#7C048C',
        '#760493',
        '#70039A',
        '#6903A1',
        '#6303A7',
        '#5D03AE',
        '#5702B5',
        '#5102BB',
        '#4A02C2',
        '#4402C9',
        '#3E01D0',
        '#3801D6',
        '#3201DD',

```

```

'#2B01E4',
'#2500EA',
'#1F00F1',
'#1900F8',
'#1300FF'
]
for i in range(total_days-len(hexcolors)):
    hexcolors.append('k')

# Number of weeks in currently studied period
for i in range(int(math.ceil(float(total_days)/float(binlength)))):
    # print "Week %s:" % (i+1)
    numberofpoints += len(observed[i])

    for location in locations:
        try:
            # Try a linear regression, assuming there are points
            # in that week
            slope, intercept, r_value, p_value, std_err =
            linregress(modelledbylocation[location][i],observedbylocation[location][i])
            tempx = [0,0.02]
            tempy = [f*slope+intercept for f in x]
            label1 =
            ax1.scatter(modelledbylocation[location][i],observedbylocation[location][i],color=hexcolors[i],s=10,marker=markers[location],label=location)
            # ax1.plot(tempx,tempy,locationcolors[location]+'-'
            ',lw=1.0)
            ax1.plot(tempx,tempy,'k-',color=hexcolors[i],lw=1.0)
            # ax2.plot([i],[slope],'ko',color=hexcolors[i])
        except ValueError:
            # For weeks with no data
            pass

    print "Number of points: %i" % numberofpoints

h,l = ax1.get_legend_handles_labels()
handles = []
labels = []
for i in range(len(l)):
    if not l[i] in labels:
        handles.append(h[i])
        labels.append(l[i])
#ax1.legend(handles,labels)
if location == 'Heimaland':
    ax1.set_ylim([0,5000])
    ax1.set_xlim([0,0.0035])
    sptitle = '(b) Heimaland'
elif location == 'Grensasvegur':
    ax1.set_ylim([0,1600])
    ax1.set_xlim([0,0.001])
    sptitle = u'(a) Grensásvegur'
#ax1.set_title('Observed vs modelled ash
resuspension',fontname='Times New Roman')
ax1.set_xlabel('NAME output (arbitrary units)')
# ax2.set_xlabel('Days past eruption end',fontname='Times New
Roman')
ax1.set_ylabel(r'Observed PM$_{10}$ output ($\mu$g/m$^3$)')
# ax2.set_ylabel('Slope of $\bar{K}$',fontname='Times New Roman')
# ax2.set_ylim([-1*10**7,1*10**7])
# for tick in ax1.get_xticklabels():
#     tick.set_fontname('Times New Roman')
# for tick in ax1.get_yticklabels():
#     tick.set_fontname('Times New Roman')
ax1.set_title(sptitle,loc='left')

print "R-squared = %s" % r**2

```

```

fig.set_tight_layout(True)
plt.show()
plt.close()

if __name__=='__main__':
    main(sys.argv[1:])

```

C.3 ***subtractglaciers_glims.py***

This Python script opens a file containing the geographic coordinates of the center of each source grid rectangle. Utilizing a polygon representing the areal extent of the glaciers of Iceland, it checks whether the center of each point source lies within an area of mapped glacier, in which case the point is removed.

It outputs a file containing only the gridded source points outside of the areal extent of the glacial polygon, and plots a Mercator projection showing the location of each of the remaining points as well as the glacial polygon itself. This script represents the second version (taking on the ‘_glims’ suffix), using an updated glacial polygon shape file from the GLIMS database (Sigurdsson 2005).

When this process was originally performed, the scaled sources file contained source points for the ash deposit from the nearby eruption of Grímsvötn in 2011. These points were subsequently removed.

```

#!/bin/python
#
# Use: Plot a 2-D map over Iceland of where the sources are being
emitted
# Author: Cameron R. Powell, IMO, November 20171101
#           with some syntax borrowed from Frances Beckett, ADAQ
(plotplume.py)
#

import matplotlib.pyplot as plt
import matplotlib.ticker as mticker
import cartopy.feature as cfeature
import cartopy.crs as ccrs
from cartopy.mpl.gridliner import LONGITUDE_FORMATTER,
LATITUDE_FORMATTER
import matplotlib
from matplotlib.colors import BoundaryNorm
import csv
import fiona
from shapely.geometry import Point,shape
from time import sleep

def main(*args):

    #--- Setup -----
--#
    countries = cfeature.NaturalEarthFeature(
        category='cultural',
        name='admin_0_countries',
        scale='10m',
        facecolor='none')

    glaciers = cfeature.NaturalEarthFeature(
        category='physical',
        name='glaciated_areas',

```

```

        scale='10m',
        #facecolor='lightblue')
        facecolor='none')

# Set up the Figure Axes
ax = plt.subplot(111, projection=ccrs.Mercator())
##TODO: Add background map?
ax.set_extent([-24, -13.5, 63.3, 66.6])
ax.add_feature(countries, edgecolor='black', zorder=2)
ax.add_feature(glaciers, edgecolor='blue', zorder=2)

# Set up the gridlines
gl = ax.gridlines(draw_labels=True,
                    linewidth=0.8,
                    alpha=0.9)
gl.xlabel_top = False
gl.ylabel_right = False
gl.xlocator = mticker.FixedLocator([-25,-23,-21,-19,-17,-15,-13])
gl.ylocator = mticker.FixedLocator([54,56,58,60,62,64,66,68])
gl.xformatter = LONGITUDE_FORMATTER
gl.yformatter = LATITUDE_FORMATTER
gl.xlabel_style = {'size': 12}
gl.ylabel_style = {'size': 12}

fc = fiona.open("glims_download_00382/glims_polygons.shp")
features = [shape(feature['geometry']) for feature in fc]

def onGlacier(lon,lat):
    for feature in features:
        if Point(lonpt,latpt).within(feature):
            return True
    return False

# Length of file minus headers, for % tracking
length = sum(1 for line in open('Sources_nooverlap_NAME_5mm.txt'))-2
with open('Sources_nooverlap_NAME_5mm.txt','rb') as f, \
open('NAME_glacier_sources_scaled_glims.txt','wb') as g:
    lon = []
    lat = []
    reader = csv.reader(f)
    writer = csv.writer(g)
    # Remove header
    writer.writerow(next(reader))
    writer.writerow(next(reader))
    i = 1
    for line in reader:
        print "Line %d of %d: %.2f%%" %
(i,length,100*float(i)/float(length))
        # Get lon and lat
        lonpt = float(str.strip(line[6]))
        latpt = float(str.strip(line[7]))
        # Check for if point is in glaciated area
        if onGlacier(lonpt,latpt):
            print "Removed point at lon:%f, lat:%f" %
(lonpt,latpt)
            else:
                lon.append(lonpt)
                lat.append(latpt)
                writer.writerow(line)
        i += 1

plt.plot(lon,lat,'r.',markersize=2,transform=ccrs.Geodetic())
plt.subplots_adjust(bottom= 0.1, wspace = 0.2)
plt.show()
plt.close()

```

```
if __name__ == "__main__":
    main()
```


Appendix D: Description of Input Files

D.1 *input.txt*

This is a headed text file containing all of the information required by NAME to properly execute the requested computations. While itself able to contain sources and met definitions, the input file for the purposes of this study and general operation instead pointed to external files for each of these requirements (see below). Also defined here are the requested output data. Multiple versions of this file were maintained, each for a separate use: daily forecasting of current resuspension events, modelling PM₁₀ concentrations at each of the appropriate monitoring locations, and modelling PM₃₂ concentrations at Drangshlíðardalur.

D.2 *sources.txt*

This text file contains a list of gridded points of latitude and longitude representing the center of 0.01° × 0.01° degree cells. Each entry contains additional information required by NAME to properly set up the particle release scheme. Within this file, each point is attributed a time of release start and time of release end. These are required to emit particles for the entire duration of the model run; actual release is handled by NAME itself, using the predefined release parameters (for volcanic ash, when the threshold friction velocity exceeds 0.4 m s⁻¹ and precipitation over the area is at a rate lower than 0.01 mm h⁻¹). These release start and end times within the sources file were automatically changed via the set of scripts developed to set up and run NAME automatically.

Various copies of this file under suffixed names were created to allow for differing source conditions: removal of source points within the glacier shape polygons, scaling of the source emission rates per areal extent, and removal of the Grímsvötn deposit points.

D.3 *MetDefnECMWF_OPER_0125_fore.txt*

This file facilitated the interpretation of NWP inputs by NAME. It included specially formatted descriptions of the various model levels and information about the fields included in each NWP met file. Both the model level and field definitions required alteration to accommodate both the past NWP data used in the study of events from 2010–2011 and also the ECMWF data itself, possessing a different file structure than that of the NWP files typically employed by the UK Met Office.